COMPUTATIONAL STUDY OF BEHAVIOR OF GAS ABSORPTION IN DATA CENTER EQUIPMENT AND ITS EFFECTS ON THE RATE OF CORROSION/CONTAMINATION

by

TEJESHKUMAR VASANTRAO BAGUL

Presented to the Faculty of the Graduate School of

The University of Texas at Arlington in Partial Fulfillment

of the Requirements

for the Degree of

MASTER OF ENGINEERING IN MECHANICAL ENGINEERING

THE UNIVERSITY OF TEXAS AT ARLINGTON

December 2014

Acknowledgements

I would like to take this opportunity to thank my thesis guide Dr. Dereje Agonafer, who was a source of inspiration to me throughout my work. I would also like to thank him for his encouragement to help me cross all the obstacles.

I would also like to thank Dr. Haji-Sheikh and Dr. Kent Lawrence for being on my thesis committee and helping me whenever I need a helping hand. I would like to thank Dr. Parabjit Singh, IBM who was a torch bearer for me in this project related to contamination in data centers. A special thanks to Ms. Sally Thompson for her immense help throughout my stay at UT Arlington.

I would also like to thank my colleagues at the EMNSPC who were as good as my family across seas. I would also like to thank Mr. Oluwaseun Awe, Mr. Betsegaw Gebrehiwot, Mr. John Fernandez and Mr. Fahad Mirza for being of great help.

Finally I would like to dedicate my thesis to my mother Mrs. Surekha Bagul who made me the person I am today. I would also like to acknowledge my father Mr. Vasantrao Bagul, my sister-in-law Mrs. Monica Bagul, my brother Maj. Pankesh Kumar Bagul and my niece Ms. Parnika Bagul for being with me in at all times and having faith in me and my work.

November 5, 2014

Abstract

COMPUTATIONAL STUDY OF BEHAVIOR OF GAS ABSORPTION IN DATA CENTER EQUIPMENT AND ITS EFFECTS ON THE RATE OF CONTAMINATION/CORROSION

Tejeshkumar Vasantrao Bagul, MS

The University of Texas at Arlington, 2014

Supervising Professor: Dereje Agonafer

The reliability of the data center equipment is being compromised as the American Society of Heating, Refrigeration and Air Conditioning Engineers (ASHRAE) recommendable psychrometric limits are stretched outside the recommendable zones. When the ambient conditions are conducive enough the humidity and the gaseous contaminants present in the data centers react with the elements of Printed Circuit Boards (PCB) at various temperatures. The products of the reaction may lead to short circuit or extra resistance to the passage of current. This poses an increased threat to the reliability of the PCB.

Contamination has become a serious problem in the developing nations like China and India where new data centers are rapidly coming

up. The heavy industrialization and vehicular activities are the major source of the contamination. The losses due the corrosion of PCB by contaminants depends on various factors like concentration of gases, amount of humidity present, time of the day, location of the data center, filtration technique used for the air-conditioning system, etc. An actual study of effects contaminants in data centers across the world would be a tedious task. Computational study saves the time as well as cost for this study.

This research study gives deeper insights of the reaction mechanism. A computational study of the reaction of copper foils (representing the PCB) placed in a Paddle Wheel Test setup would be carried out. A Paddle Wheel Test setup gives us the flexibility to test various gases, that could pose a threat to data center equipment, without disturbing the actually data center servers. A reaction of hydrogen sulfide and sulfur dioxide on copper in the presence of humidity will be carried out in this study.

TABLE OF CONTENTS

List Of Figures

List Of Tables

Chapter 1

Introduction

1.1 Contaminants

The atmosphere of the earth consists of various gases .Some of the constituents of the atmosphere are Nitrogen, Oxygen, Argon, Carbon Oxide, Neon, Methane, Helium, Krypton, Hydrogen, Xenon, etc. [1]. The individual percentage of gases is as shown in Table 1

Table 1 Constituents of Atmospheric Gases [1]

Name	**Symbol**	**Percent by Volume**
Nitrogen	N_2	78.084%
Oxygen	O_2	20.9476%
Argon	Ar	0.934%
Carbon Dioxide	CO_2	0.0314%
Neon	Ne	0.001818%
Methane	CH_4	0.0002%
Helium	He	0.000524%
Krypton	Kr	0.000114%
Hydrogen	H_2	0.00005%
Xenon	Xe	0.0000087%

Many of these gases occur naturally in nature (Which are called the organic gases), while many are a product of human activities such as industrialization, combustion of fossil fuels, burning biomass for producing energy and so on (which are categorized as inorganic gases)[2]. These gases can be further categorized as per their corrosivity, flammability, toxicity [3]. Excessive inorganic corrosive gases pollute the atmosphere and cause health concerns as well as hindrance to the human activities. Reliability of the data centers has been increasingly compromised in the past years due to some of these inorganic corrosive gases and particulate matter. The gases which might have an adverse effect on the reliability of data center equipment are called as Gaseous contaminants. Most of the data centers are designed well and are in areas with relatively clean environments, and most of the contamination is benign. Therefore most of the data centers do not face gaseous or particulate contamination-related information technology (IT) equipment failures. A small number of data centers, however do. According to the major IT equipment manufacturers, the number of data centers with contamination-related failures is on a rise, though their numbers remain quite small [4].

Typical examples of particulate contaminants are synthetic vitreous fibers, asbestos, environment tobacco smoke, combustion nuclei, nuisance dust, smoke, fumes, mists etc. [5]. The particulate contaminants are one of the leading cause of failures IT equipment. These contaminants settle on the surface of the Printed Circuit Boards (PCB) as time passes. Many of the particulate matter are conductive to electricity. When the particulate matter accumulates and links the adjacent buses or solder joints on the PCB, it gives rise to an electric short as shown in Figure 1

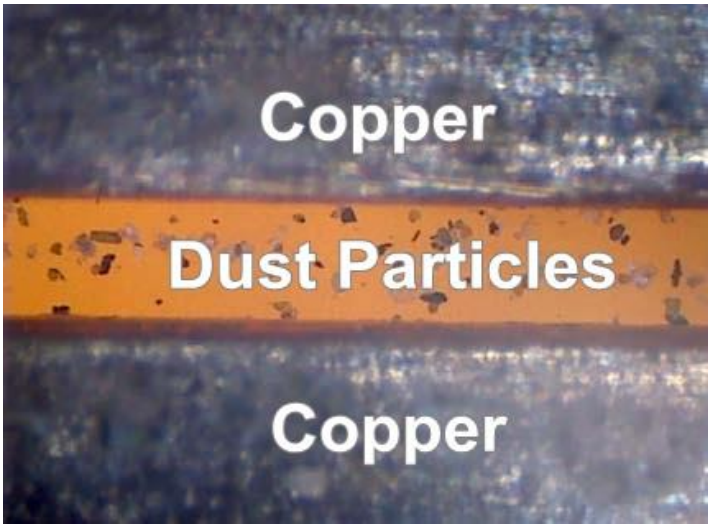

Figure 1 Magnified view of Dust Particles on a PCB [6]

The gaseous contaminants undergo a chemical reaction with the elements of PCB. The products of the reaction give rise to surface deposition on the PCB. These products, as the gradually increase, short the adjacent buses or solder joints as shown in Figure 2

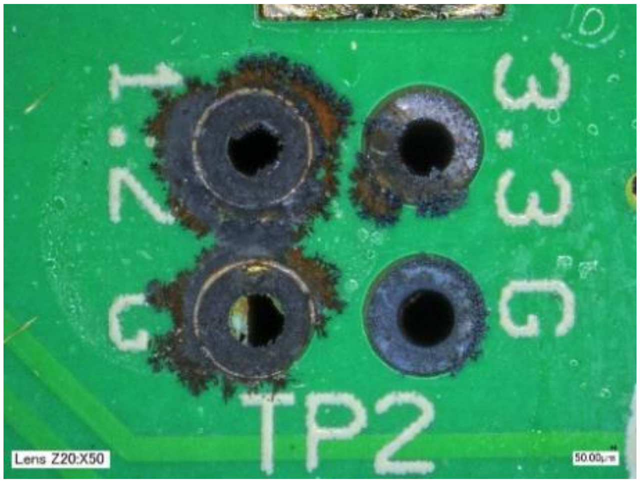

Figure 2 Short Due to the Mixture of Gaseous Contaminants

Sulfur bearing gases, such as Sulfur Dioxide (SO_2) and Hydrogen Sulfide (H_2S), are the most common gases causing corrosion of electronic equipment [4]. But the gaseous contaminants are not limited to these gases. Nitrous Oxides (NOx), active Sulfur compounds (elemental sulfur), inorganic Chlorine compounds (Chlorine (Cl_2), Chlorine Dioxide (ClO_2), Hydrogen Chloride (HCl), etc.), photochemical species (Ozone (O_3)), and strong oxidants have also been noticed to have an adverse effect on the IT equipment [7].

1.2 Corrosion

Corrosion is a naturally occurring phenomenon commonly defined as the deterioration of a substance (usually a metal) or its properties because of a reaction with the environment. Like other natural hazards such as earthquakes or severe weather disturbance, corrosion can cause dangerous and expensive damage to everything from IT equipment, automobiles, home appliances, and drinking water systems to pipelines, bridges, and public buildings.

Corrosion can occur in two general ways; over the entire surface of the metal (Generalized Corrosion), or in local spots or areas (Localized Corrosion). Generalized Corrosion, typically never happens, aside from in acidic conditions. This uniform corrosion over the entire surface of the metal is rare and leads to overall thinning which has little effect outside of fatigue and stress conditions. Localized Corrosion is the most common, and most detrimental, form of localized corrosion is pitting. Pitting is when the attack happens in one single location on the surface and creates a pit, or small cavity, in the metal. This type of corrosion attack is hard to prevent, engineer against, and often times difficult to detect before structural failure is met due to cracking. Pipes are often compromised due to pitting [21].

According to the current U.S. corrosion study, the direct cost of metallic corrosion is $276 billion on an annual basis. This represents 3.1% of the U.S. Gross Domestic Product (Figure 3)[8]

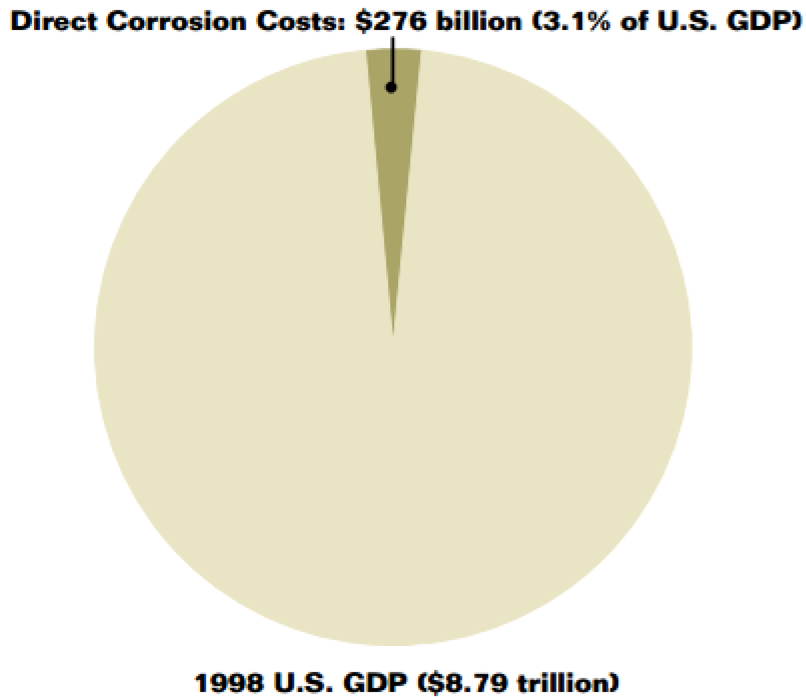

Figure 3 The Impact of Corrosion on the U.S. Economy [8]

Other studies done in China, Japan, the U.K., and Venezuela showed similar to even more costly results, leading to an estimated worldwide direct cost exceeding $1.8 trillion [9]. These losses for the geographical area of the U.S. can be further divide as shown in Figure 4

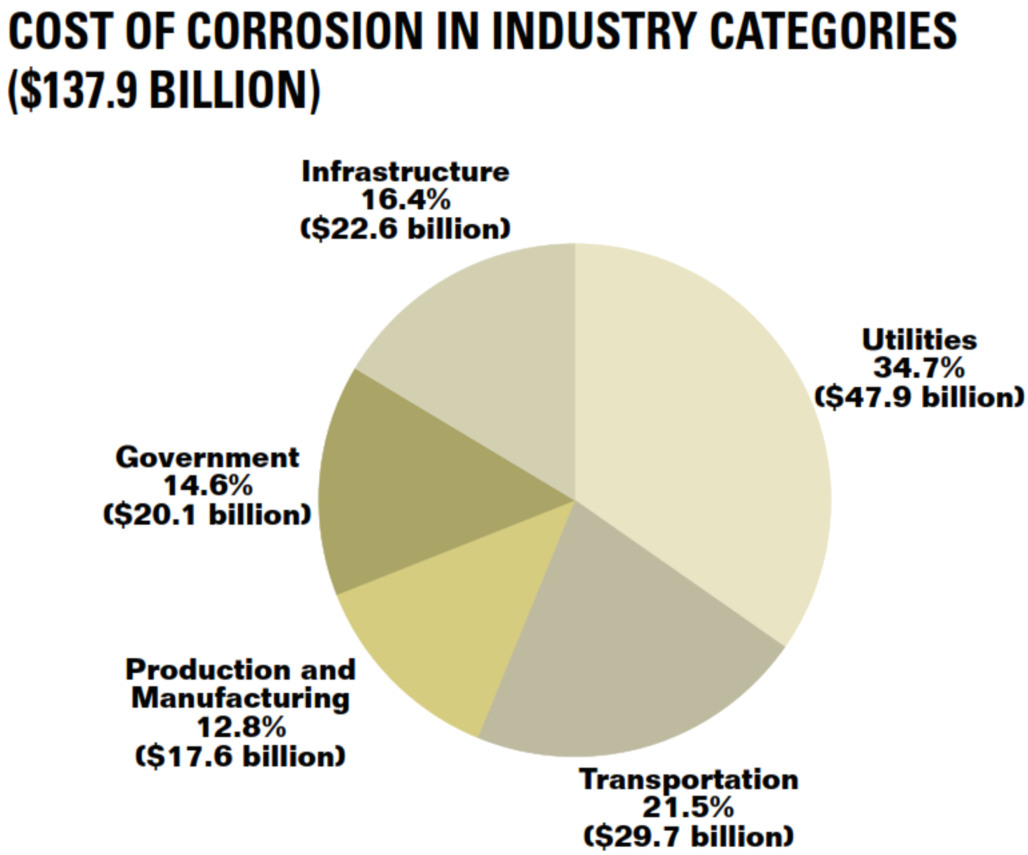

Figure 4 Percentage and dollar contribution to the total cost of corrosion for the five sector categories analyzed [8]

The data centers are categorized under the Utilities, which as seen in Figure 4 has the maximum percentage of loss due to corrosion. The utilities are further sub categorized as Electrical Utilities and Telecommunications, Drinking Water and Sewer systems, and the Gas distribution related corrosion losses. In these subcategories data centers come under the electrical utilities and telecommunication subcategory. Components of data centers like hard drives, printed circuit boards, etc.

were considered for this study. These losses were studied to be around $6.9 billion. Figure 5 shows us a pie chart for the subcategories in utilities.

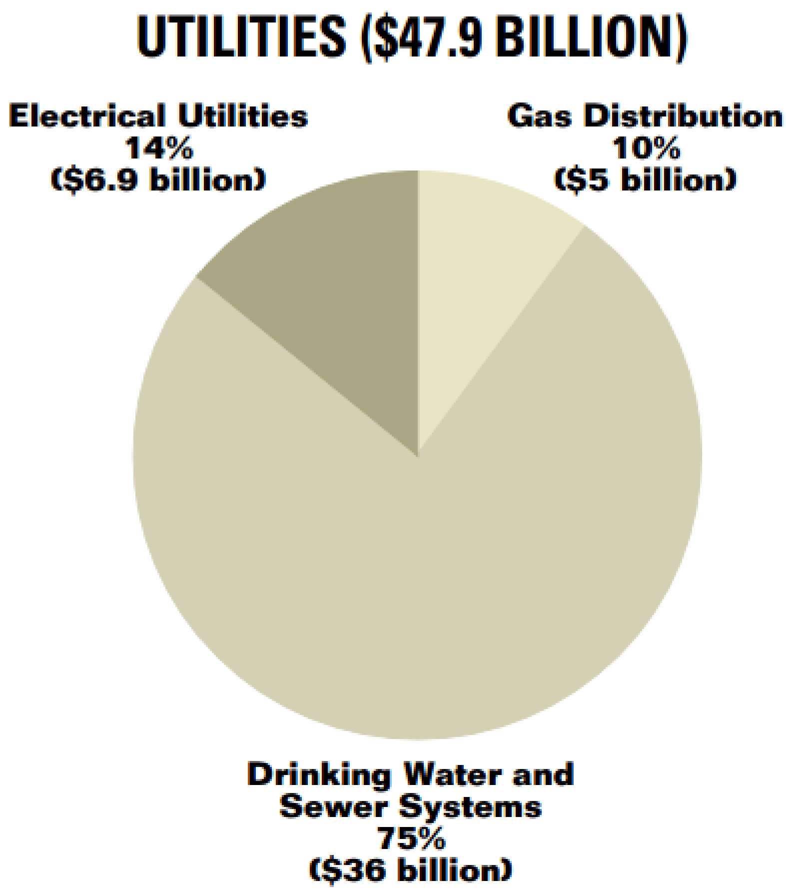

Figure 5 Annual cost of corrosion in the utilities category [8]

Corrosion is a electrochemical process and can occur in two general ways; over the entire surface of the metal (Generalized corrosion), or in local spots or areas (Localized Corrosion).

The most common corrosion that is encountered is the corrosion of iron alloys, particularly steel. This is a process where the water molecules interact with the iron (ferrous) to form ferrous oxide thus giving rise to corrosion. But corrosion is not restricted to iron alloys. It has been encountered in various other metals and non-metals such as Copper, Silver, Mercury, Lead, Tin, Zinc, etc.

Corrosion is possible in small daily use products and may range all the way to gigantic products. As seen from the amount of economic resources wasted on this phenomenon in nature it needs to be studied more closely.

Figure 6 Example of Pitting Corrosion in pipes [22]

Figure 7 Example of Fatigue Corrosion [22]

1.3 Corrosion due to gaseous contaminants in data center equipment

On 27 January 2003 the European Union (EU) in its Restriction of Hazardous Substances (RoHS) compliance stated the ill effects of using

Lead in various materials of day to day use [15]. Lead had been a major element of IT equipment till then [16]. As a part of this compliance the IT equipment manufacturers had to drop out the use of Lead in the solders used in the IT equipment. This made them to shift their focus to elements like copper and silver. Copper and silver are some of the best metals that are ductile, malleable and also have good electrical conductivity [17] [18]. But these advantages come with some disadvantages. Copper and Silver have the properties of forming sulfides and sulfates when they come in contact with the Sulfur Bearing gases in the atmosphere [19], thus compromising the reliability of IT equipment.

Data Center is a facility used to house IT systems and associated components, such as telecommunications and storage system. Driven by rising power densities and heat levels, data center cooling strategies have changed dramatically over the time. Until recently, most cooling schemes relied on so-called ‘chaos’ air distribution methodologies, in which perimeter computer room air conditioning (CRAC) units pumped out massive volumes of chilled air that both cooled IT equipment and helped push hot exhaust air towards the facility’s return air ducts. Chaos air distribution however, commonly results in wide range of significant insufficiencies, including recirculation, air stratification, bypass air, etc. Eager to combat these inefficiencies and keep pace with steadily climbing data center temperatures, business often adopt the hot aisle/ cold aisle rack orientation arrangements, in which only hot air exhausts and cool air intakes face each other in a given row of server racks [11].

Air side economization is one of the ways to maintain the temperature of data centers with the hot aisle and cold aisle method as shown in Figure 8

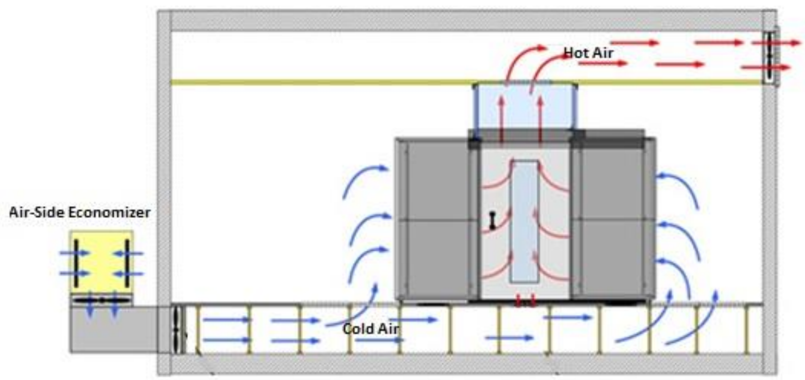

Figure 8 Air-Side Economizer [12]

The Air-Side Economizers work on the principle of free air cooling which implements outside ambient air as the working fluid. The American Society of Heating, Refrigeration and Air Conditioning Engineers (ASHRAE) in its white paper titles “2011 Gaseous and Particulate Contamination Guidelines for Data Centers” recommend the use of MERV 11 or MERV 13 filters to maintain the levels of contaminants in data centers.

Minimum efficiency reporting value (MERV) rating is a measurement designed by the ASHRAE to rate the effectiveness of the filters. Table 2 gives a brief view of various MERV filters and their corresponding use.

Table 2 MERV Rating and Applications [13]

MERV	Minimum Particle Size	Typical controlled contaminants	Typical Applications
1-5	>10.0µm	Pollen, dust mites, cockroach debris, sanding dust, spray paint dust, textile fibers, carpet fibers, Mold, spores, dust mite debris, cat and dog dander, hair spray, fabric protector	Residential window AC units

Table 2 Continued

6-10	10.0µm – 4.0µm	Dusting aids, pudding mix, Legionella, Humidifier dust, Lead dust, Milled flour, Auto emission particulates, Nebulizer droplets	Better residential, general commercial, industrial workspaces
11-15	4.0 µm -0.3µm	Bacteria, droplet nuclei (sneeze), cooking oil, most smoke and insecticide dust, most face powder, most paint pigments	Data centers, hospital & general surgery rooms
16-20	<0.3µm	Virus, carbon dust, smoke	Electronics & cleanrooms

In a typical Indirect Air-Side Economizer setup can be graphically illustrated as shown in Figure 9. The MERV filter is located at the location pointed out as Outside Air Filter in the Figure 9

Figure 9 Indirect-Evaporative Air-Side Economizer Unit [14]

Despite of improved filtration techniques contaminants find a way into the data centers.

The American Society of Heating, Refrigeration and Air Conditioning Engineers' (ASHRAE) TC9.9 committee has laid guidelines for maintaining the thermal conditions of data centers. The TC9.9 committee in its book titled "Thermal Guidelines for Data Processing Environments, 3rd Edition" has specified certain recommendable envelopes for data center to operate. Figure 10 gives the recommendable and allowable environmental conditions for electronic equipment.

As seen from the psychrometric chart the recommended range for temperature is 18ºC to 27ºC and for humidity is up to 60%. These conditions are conducive enough for corrosion to occur on the IT equipment. Thus, the air entering the data center from Air-Side economizers pose a threat to the IT equipment in there. Gaseous contaminants like Sulfur Dioxide (SO_2), Hydrogen Sulfide pose similar kind of threat to the reliability of elements of copper and Silver which make up a major part of the solder on Printed Circuit Boards i.e. data center equipment.

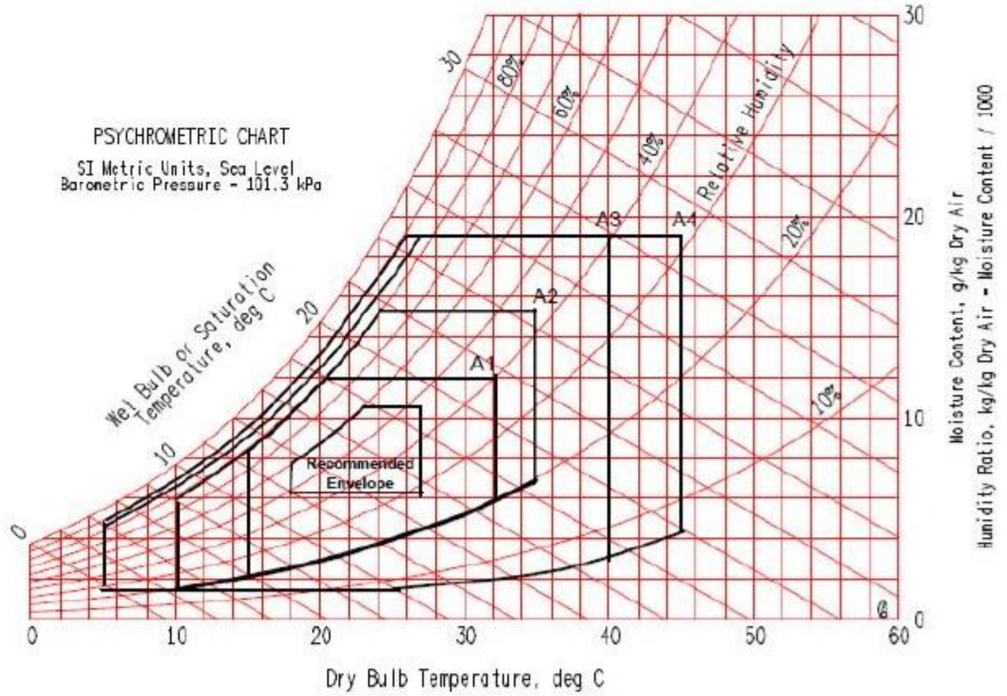

Figure 10 Recommended and allowable environmental conditions for electronic equipment (ASHRAE, 2012)

In many cases the sulfur bearing gases (contaminants) react with the copper and silver on the PCB. The products of these reactions give rise to surface deposition on the PCB. Many a time these products case adjacent solder holes or bus lines to short as shown in Figure 11

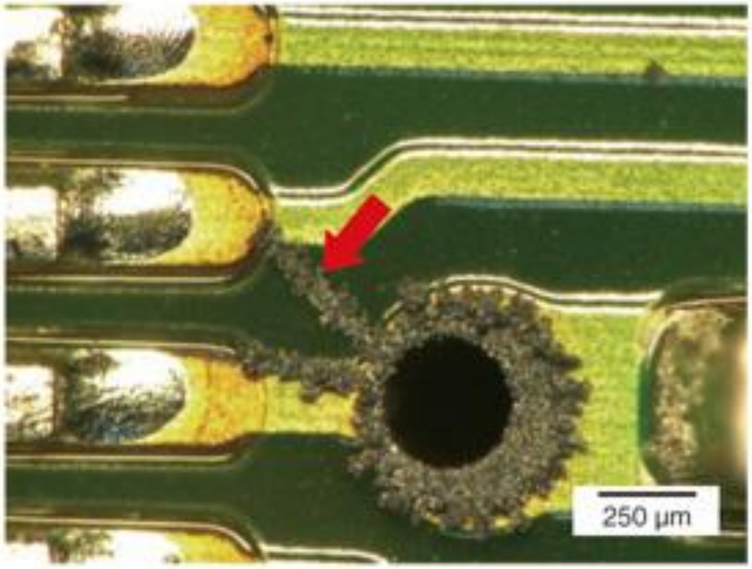

Figure 11 Short in adjacent solder hole and bus line as a result of surface deposition [20]

Problems like these when grow give rise to loss on time and economic resources. Thus a study in this area would give deeper insights of how the gaseous contaminants would play a role in reliability of IT/data center equipment.

1.4 Motivation

The paper titled “The Influence of Oxide Layers on Initial Corrosion behavior of Copper in air containing water vapor and sulfur dioxide” by Jun Itoh, Takeshi Sasaki, Toshiaki Ohtsuka from Hokkaido University, Japan has discussed the effects of sulfur dioxide on Copper plates in the presence of water vapor (relative humidity). Corrosion rate of copper at different surface states of specimen were prepared by different surface finishing methods, and the surfaces under corrosion test in air containing water vapor of 78%-83% Relative Humidity (RH) and SO_2 of 16-23ppm were investigated [23].

The paper is focuses specifically towards the corrosion of microelectronic systems that contain copper as one of their elements. Sample of copper plates (12x22x1.0mm) were prepared for this experiment. These plates were then exposed to SO2 gas at varying RH at room temperature. The products of the reaction were at studied at the end of the experiment, with the help of Infrared Spectrometer. The main products were found out to be Copper Sulfate ($CuSO_4$) and Chevreul's salt ($CuSO_3Cu_2SO_3$).

These products can be followed up by the following chemical reaction:

$$Cu+SO_2+2H_2O \rightarrow CuSO_4 + 2H_2$$

Along with the SO2, H2S has also been found out to be equally harmful to the reliability of IT equipment. In addition to SO2, effects of H2S (not studied in the cited paper) would also be studied in this thesis study. A suitable chemical equation for effect of H2S can also be given as shown below:

$$Cu+H_2S+4H_2O \rightarrow CuSO_4 + 5H_2$$

1.5 Paddle Wheel Test Setup

Scientists and researchers in the field of corrosion, due to contamination in data center, have developed an innovative test setup for testing the rate of corrosion on IT equipment. A Paddle wheel Test setup (also called as Flowers of Sulfur Chamber) is a test setup used to measure the rate of contaminants in PCBs without disturbing the operating machinery of any data center. It is an accelerated test setup of studying the effects of sulfur [19].

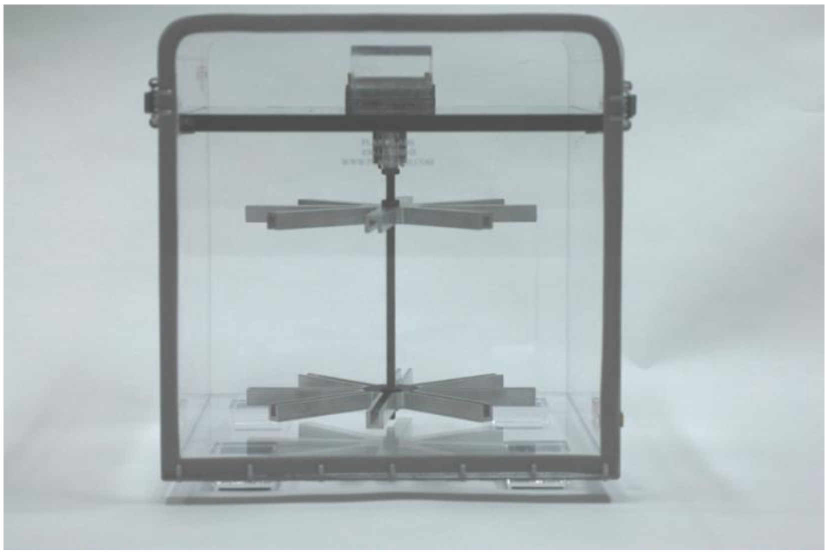

Figure 12 Paddle Wheel Test Setup

As seen in Figure 12 , the Paddle Wheel Test Setup is 1 foot x1 foot x1 foot cube structure. The front side of the Paddle Wheel Test Setup's front side has a door. The entire setup is air-tight. Only one opening is facilitated for the motor wiring as seen in Figure 13 [19].

Figure 13 Opening for Motor Wiring

The gear train starts with a DC gear-motor. The motor has a maximum of 50rpm speed. The shaft of the motor is connected to the central shaft through a coupling mechanism. The central shaft is runs from the coupling to the end (it does not touch the bottom). The central shaft is a solid shaft made out of steel. Its diameter is 1 centimeter and the length of the shaft is 9 inches [19].

Two aluminum carousels are mounted on the central shaft. Thus the rotary motion of the motor is transferred from the shaft to the carousels. The carousels are machined to fit test specimen into them. The diameter of the carousel is 8 inches as seen in Figure 14. A total of eight test specimen can be mounted between the carousels. In the actual test four copper and four silver foils were mounted on alternate carousels. These foils were used as elemental representation of the copper and silver on the Printed Circuit Boards [19].

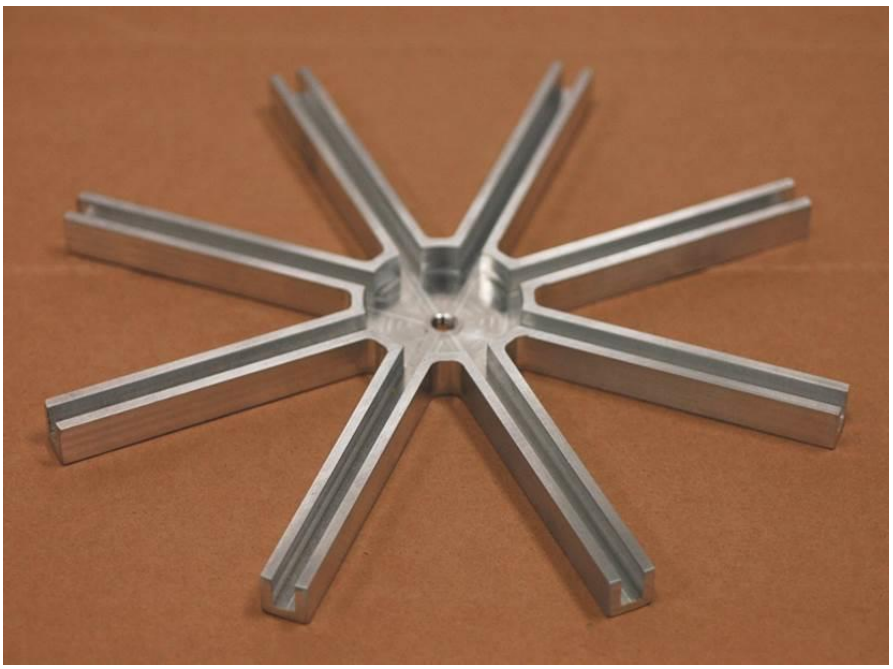

Figure 14 Carousel

This test setup used elements sulfur (S_8) as the contaminant in powder form. The S_8 was kept in two petri dishes. These petri dished were kept inside the test setup on the bottom face. Two petri dishes containing Potassium Chloride (KCl) salt were also kept along with the S_8 dishes. The KCl salt was used to introduce relative humidity in the test setup. The whole test setup is then kept in an environmental test chamber to maintain the temperatures of the test [19].

As the motor was switched on the S_8 in the petri dishes is displaced due to the motion of the foils placed between the carousels. This S_8 diffuses in the air in the test setup. With the increase in time the foils start absorbing the S_8. Thus, layers of reaction products are formed on the foils. The after products of the reaction were found out to be Copper Sulfide (Cu_2S) in this case.

Thus the corrosion products were further studied under various temperature and relative humidity conditions.

In this thesis study the actual test setup will be solid modeled and checked for reactivity of gases like H_2S and SO_2 on copper foils in the presence of relative humidity (as per the motivation). This thesis study would be analogous to that of the motivation study but would also be modified for present data center condition as per ASHRAE TC9.9 standards.

Chapter 2

Solid Model and Meshing

2.1 Solid Model

2.1.1 Cabinet

As per the actual experimental model the cabinet is designed in SolidWorks. The dimensions of the solid model are same as that of actual model. The cabinet is also provided with a door to make the entire air thigh.

As discussed earlier the actual setup used petri dishes containing the contaminants and salt for maintaining the relative humidity. For this thesis study the petri dishes are eliminated. Instead four inlets and four outlets are introduced on the top and bottom faces of the cabinet respectively. The diameter of all the inlets and outlets is 10mm. An extra space has been made to mate the central shaft in the cabinet's solid model as seen in Figure 15

We can eliminate the motor and locking mechanism as the Computational Fluid Dynamics pre-processor gives us the flexibility to assign each part its rotation speed. This would be discussed in the further section of this report.

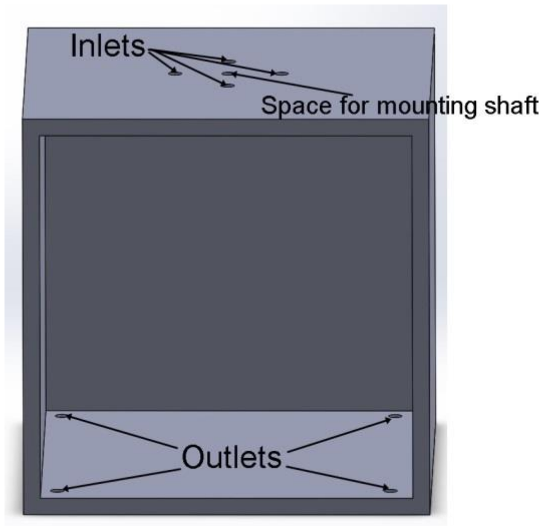

Figure 15 Cabinet Solid Model

2.1.2 Central Shaft

The central shaft in the actual test setup runs from the motor locking mechanism to the end. It also houses two locking mechanism for the carousels. The carousels are mated in the assembly of the solid model. Thus, eliminating the need of a locking mechanism on the central shaft Figure 16 gives the idea of the solid modeled shaft. The diameter of the shaft is 10mm while its length is 9”.

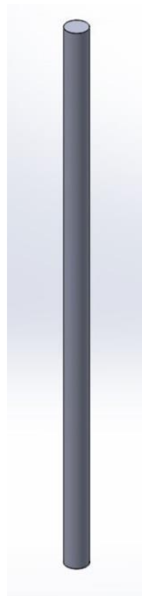

Figure 16 Central Shaf

2.1.3 Carousel

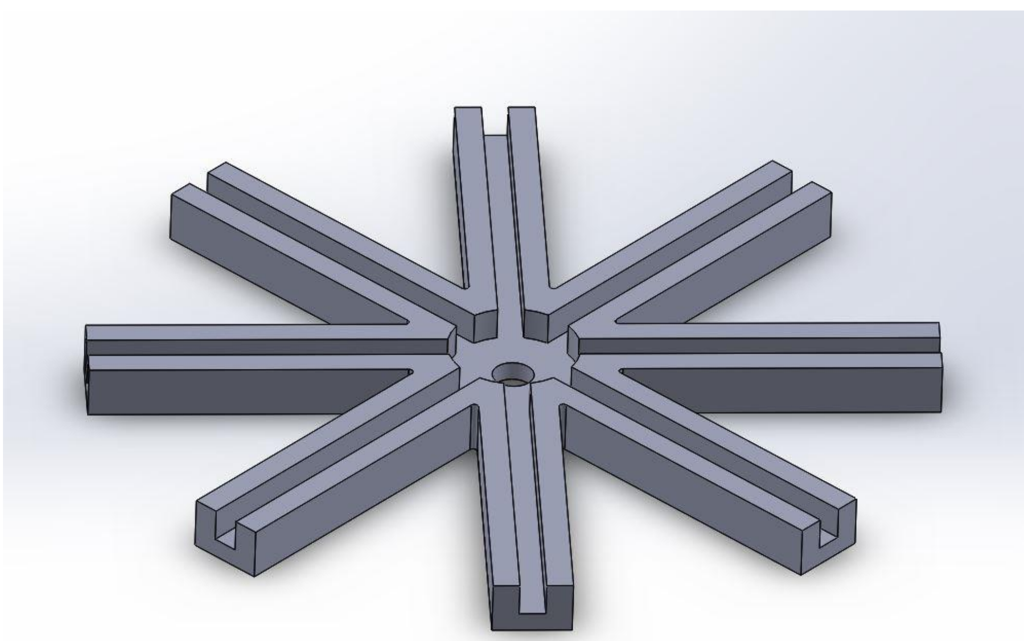

Figure 17 Carousel

A set of two carousels are mounted on the central shaft. The carousels act as a medium to transfer the rotational motion from the central shaft to the foils. The carousels have an external diameter of the carousels is 8”. As seen in Figure 17 the carousels have eight faces to hold eight individual foils.

The distance between the top and bottom carousel is 6.7”. In the solid model assembly the carousels are mated with the central shaft.

2.1.4 Foil

The foils are the last part of the rotary motion. The dimensions of the foils are 6.7”x1.6”, while the thickness is 10mm. As the rotary motion is imparted to the foils the air in the test setup is displaced.

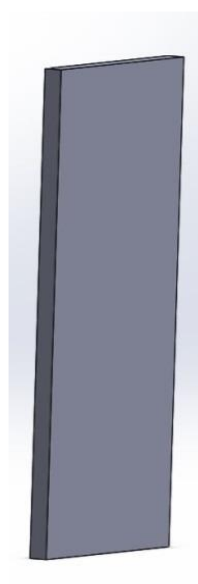

Figure 18 Foil

2.1.5 Assembly

All the parts (which consist of 1 Cabinet, 1 Central shaft, 2 Carousels and 8 Foils) are mated and assembled in SolidWorks. Figure 19 illustrates the assembled test setup.

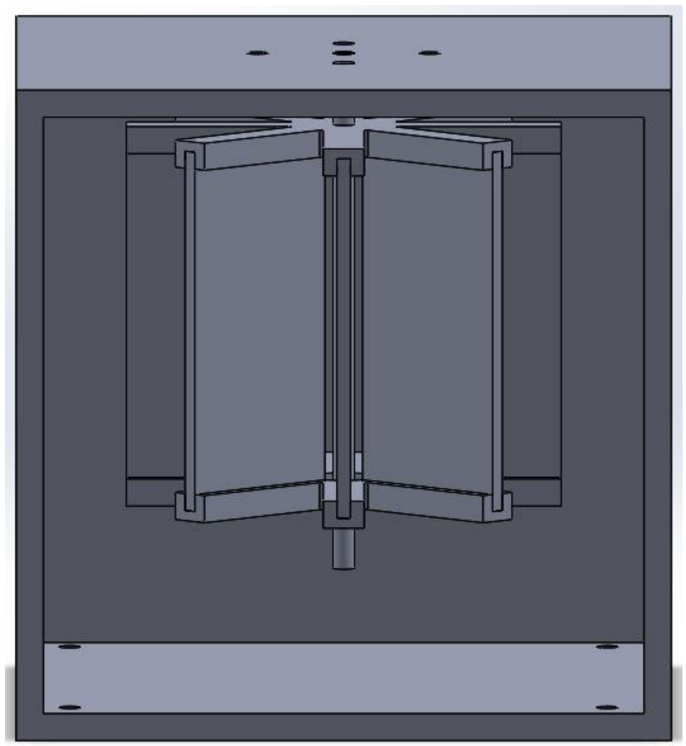

Figure 19 Assembled test setup as displayed in SolidWorks

2.2 Mesh

The solid model is imported to ANSYS WorkBench for further analysis. A mesh model of the solid model is developed in the ANSYS Mesh Tool. After various trials and mesh sensitivity checks one optimized mesh was selected for this study. The meshed model is a free mesh which gave the chemical reactions to be distributed evenly over the surfaces (discussed in subsequent sections). The final meshed model has tetrahedral elements [32].

While setting up the details of mesh “CFD” is selected in the physical reference while, “Fluent” is selected in the solver preference. This helps the mesh tool to generate a mesh to be analyzed in ANSYS Fluent. The Relevance is set to +50. The relevance allows us to control the fineness of the mesh for the entire model. We can indicate a preference towards high speed (-100) to high accuracy (+100) as per our modeling needs [32].

The Advanced Size Function is set to “Proximity and Curvature” to produce an optimized results at the flow when is curves at the boundaries. The “Relevance Center” that sets the gauge of the Relevance slider control is set to “Fine”. A “medium” smoothing is set for the model. The “Smoothing” function attempts to improve the elemental quality by moving location of nodes with respect to surrounding nodes and elements [32].

The “Transition” is set to “Slow”. This affects the rate at which adjacent cell will grow. Slow produces smooth transitions while Fast produces more abrupt transitions. “Span angle center” which sets the goal for curvature based refinement is set to “Fine”. The mesh is subdivided in curved regions until the individual elements span a particular angle. This mesh has a span angle of 13.5º which comes under the fine choice [32].

The rest of the settings remain same and a mesh is generated. The meshed model as seen in Figure 20 has 2,925,393 elements and 651,898 nodes.

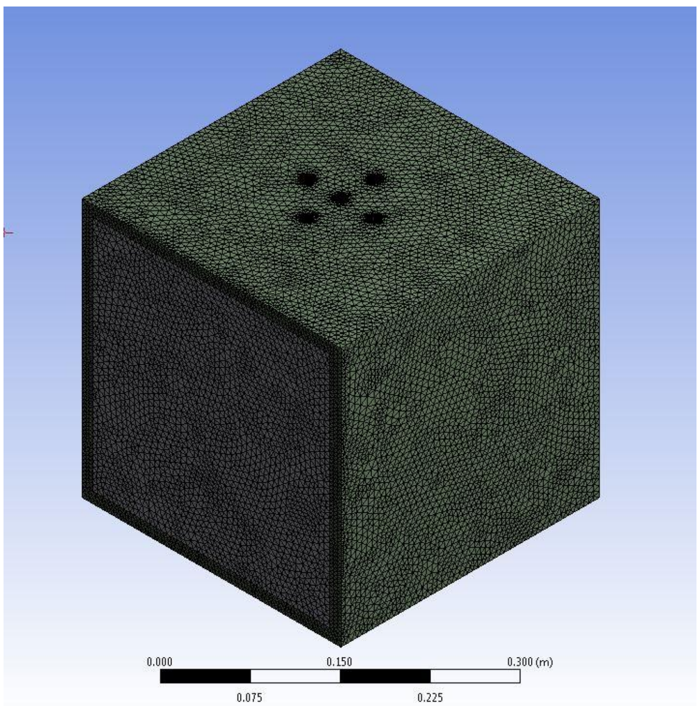

Figure 20 Meshed Model

Chapter 3

Computational Fluid Dynamics (CFD) analysis

3.1 Introduction to CFD

CFD deals with the numerical simulation and analysis of fluid flow, heat transfer characteristics and pressure characteristics. CFD uses numerical methods to predict, simulate and analyze distribution of velocity, pressure, temperature and other variables throughout the calculation domain. The calculations in CFD are based on boundary conditions and the calculations are done in a computer. CFD is used for various applications such as data center industries, system with high heat loads, telecommunication industry, and several more [24].

CFD is a bridge between pure theory and pure experiment. CFD discretize the problem based on numerical parameters to solve the problem. Experimental work is costlier than CFD analysis. When compared to conducting and experiment, CFD is very fast as we can simulate various cases in specified time period. A numerical prediction is used for the generation of a mathematical model which represents the physical domain of interest to be solved and analyzed.[24]

3.2 Governing Equations

The four differential equations namely conservation of mass, conservation of momentum, conservation of energy and conservation of chemical species commonly known as governing equations are used to solve the numerical solution for heat transfer and fluid flow based problems.

The conservation of mass equation is given by:

$$\frac{\partial \rho}{\partial x} + \nabla(\rho u) = 0$$

The conservation of momentum equation is given by:

$$\frac{\partial}{\partial t}(\rho u) + \nabla(\rho u u) = \nabla(\mu . \mathrm{gardu}) - \frac{\partial p}{\partial x} + B_x + V_x$$

The conservation of energy equation is given by:

$$\nabla(\rho u h) = \nabla(k. gradT) + S_h$$

The conservation of chemical species equation is given by:

$$\frac{\partial}{\partial t}(\rho Y_i) + \nabla(\rho \vec{V} Y_i) = -\nabla J_i + R_i + S_i$$

3.3 Global Computation Domain

The governing equations are solved in the computational domain. The control volume is defined as the closed volume within a finite region of flow. The boundary conditions for the solution domain are fixed to obtain the solution of the equations. The boundary conditions are ambient temperature, mass flow at inlet and outlet, fluid viscosity, density, velocity, pressure, and other environmental conditions. The major steps in CFD is defining the geometry of the problem, dividing the volume into discrete cells also called as meshing, applying boundary conditions and finally solving the governing equations [24].

In the present study the tool ANSYS Fluent is used for its capability of solving the species transport reaction and very well defined post processing. Mixing and transportation of the chemical species can be solved by ANSYS Fluent by solving the conservation equations. Chemical species reaction and mixing along with surface deposition/ reaction models are present in ANSYS Fluent. Free surface and multiphase models for gas-liquid, gas-solid, and liquid-solid flows, steady-state and transient flows, inviscid, laminar and turbulent flows, ideal and real gases, convection, radiation and heat transfer are few more capabilities of the ANSYS Fluent.

3.4 Turbulent Modeling

The type of the flow can be laminar, transient or turbulent depending on the Reynolds number. Turbulent flow is defined as a flow regime characterized by irregular fluctuations in all directions [25].

When the Reynolds number is less than 2300 the flow is laminar. When it ranges between 2300 and 4000 the flow is transient while turbulent when more than 4000.

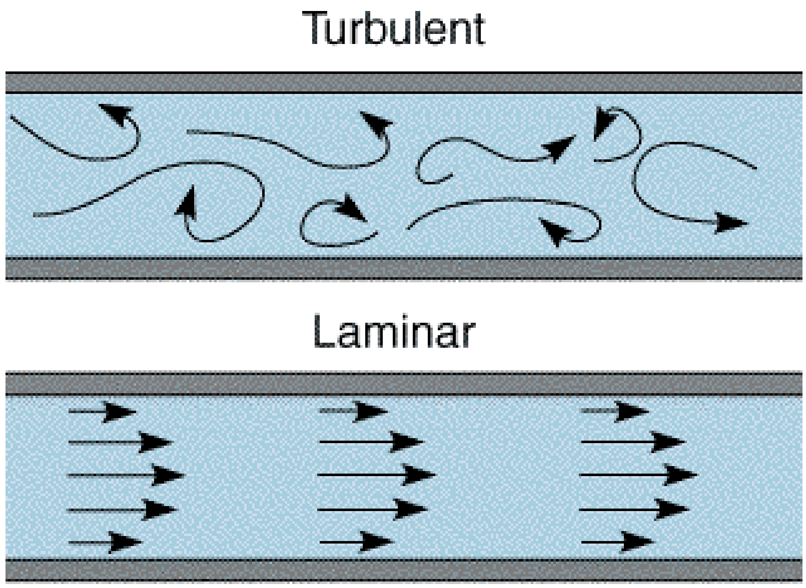

Figure 21 Graphical representation of laminar v/s turbulent flow [26]

3.4.1 K-Epsilon Turbulence model

K-Epsilon turbulence model is also commonly known as two equation model and is widely used for turbulent flow modeling. This model solves using two variables, the kinetic energy of turbulence (k) and the dissipation rate of kinetic energy of turbulence (e). Two transport equations namely Kinetic energy of turbulence (k) and the dissipation rate of kinetic energy of turbulence are solved [27]. In the present study K-Epsilon turbulence model is used. The following are the transport equations [28]:

$$\frac{\partial(\rho k)}{\partial t} + \frac{\partial(\rho k u_i)}{\partial x_i} = \frac{\partial}{\partial x_i}\left[\left(\mu + \frac{\mu_t}{\sigma_k}\right)\frac{\partial k}{\partial x_i}\right] + G_k + G_b + - \rho\varepsilon$$

$$\frac{\partial(\rho\varepsilon)}{\partial t} + \frac{\partial \rho\varepsilon u_i}{\partial x_i} = \frac{\partial}{\partial x_i}\left[\left(\mu + \frac{\mu_t}{\sigma_k}\right)\frac{\partial \varepsilon}{\partial x_i}\right] + C_{1s}\frac{\varepsilon}{k}\left(G_k + C_{3s}G_b\right) - C_{2s\,\rho}\frac{\varepsilon^2}{k}$$

3.5 Preprocessor Setup

The meshed model is imported to ANSYS Fluent. A Mesh check is performed for the effectiveness of the incoming mesh. The maximum cell skewness of the mesh is maintained below 0.98 for better solution as a rule of thumb [31].

The average aspect ratio of the imported paddle wheel test setup solid model is 1.72.

In both, Density based solver and Pressure based solver momentum equations are used to get the velocity field. Controlled volume based technique is used in both the solvers. The governing integral equations for conservation of mass and momentum, energy and scalars are solved by both the solvers. Algorithm that belongs to projection method is employed by the pressure-based solver. The density based solver solves the governing equations simultaneously [32]

A decoupled chemistry calculation starts from converged steady-state solution. The solution can be obtained from models like species transport, non-premixed, partially-premixed. The premixed combustion model, valid for turbulent, subsonic flows is available with the pressure based solver. For the present case steady state pressure based solver is used.

In the chemical species model energy is turned on as the energy is employed for the species reaction to take place. For the flow type as K-Epsilon turbulent model is chosen. The species transport model is activated. The local mass fraction of each species is predicted by ANSYS Fluent, by taking into consideration the convection diffusion equation for the specie. The mass fraction of the species must be unity, for which reason the Nth mass fraction is determined as one minus the sum of the N-1 solved mass fraction. The Nth specie is the one in abundance so it's chosen last [32]. Several elementary physic-chemical processes like chemical reaction and adsorption of gas-phase species on the surface, adsorption of gases from the surface back to the gas phase takes place while modeling the reaction.

The reaction rate of gas-phase reaction is based on basis of volumetric and rate of destruction and creation of chemical species in the species conservation equation. The source and sink of the chemical species in gas phase as well as on the reacting surface is created by wall surface reactions. The rate of adsorption and desorption in surface reaction is governed by the chemical kinetics and diffusion to and from the surface [31].

There is certain loss of mass due to the deposition reaction of the specie for which the mass reaction is enabled in the model. The robustness and the convergence speed is controlled by the aggressiveness factor, by varying the value between 0 to 1, where 0 is most robust resulting in slow convergence. For this study the aggressiveness factor is set to 0.5 by trials and optimizing the results. The effect of the enthalpy transport due to the species diffusion in the energy equation is accounted by the diffusion the diffusion energy source contributing to energy balance for the case of Lewis numbers far from the unity. Stefan-Maxwell equation is activated by the Full Multicomponent Diffusion, which computes the diffusive fluxes of all species in the mixture to all concentration gradients. Heavy molecules are diffused less rapidly and light molecules are diffused more rapidly toward heated surfaces by Thermal Diffusion [31].

3.5.1 Material Properties

Every species involved in the reaction has to be defined for ANSYS Fluent to take into consideration while simulating the reaction. Properties for the mixture material and also for its constituent species are to be defined. The species involved in the reaction has to be defined as fluid material. The mixture material is the set of the species involved in the reaction and the list of rules governing their interaction. The mixture material consists of the constituent species defined as fluid materials, along with the physical properties like density, viscosity, specific heat, etc. It also has the diffusion coefficients for individual species in the mixture. Many common mixture materials are stored in the ANSYS Fluent data base, but if the desired mixture material is not present in the data base it can be defined [31].

The present thesis study two separate CFD problems are solved for two different chemical reactions. The following are the chemical reactions that we would be using for our study:

$$Cu + H_2S + 4H_2O \rightarrow CuSO_4 + 5H_2$$

$$Cu + SO_2 + 2H_2O \rightarrow CuSO_4 + 2H_2$$

The material properties of Cu, H_2S, SO_2, H_2O and H_2 are defined in the ANSYS Fluent database, thus copied from the database for the analysis. $CuSO_4$ is not defined in the ANSYS Fluent database. The individual properties for the same are found out by literature study.

In the present study few properties are defined as Kinetic Theory as the ideal gas law is enabled. By choosing the Kinetic Theory the ANSYS Fluent compute using the empirically based expression and no further inputs are needed. The Characteristic length and Energy parameters have to be defines when using Kinetic theory along with Degrees of freedom if required.

The individual that take part in the chemical reaction are specified as gas-phase species, solid species or site species as per their role in the reaction. The gas phase species include all the gases involved in the reaction no matter whether as source or product. The site species include the species present on the site involved in the chemical reaction. Solid species are usually the products or surface deposits that occur after the chemical reaction.

The Characteristic length and Energy parameters for the solid materials are always 0 and also the degree of freedom is 0. The entropy and enthalpy are defined according to nature of the reaction. Table 3 gives the details of the individual properties of each species that has been used in this study.

Table 3 Material Properties [1] [31] [33]

Name	Copper	Hydrogen Sulfide	Sulfur Dioxide	Water Vapor	Copper Sulfate	Hydro-gen
Type of Species	Site	Gas-Phase	Gas-Phase	Gas-Phase	Solid	Gas-Phase
Chemical Formula	Cu	H_2S	SO_2	H_2O	$CuSO_4$	H_2
Specific Heat (j/kg-k)	385	Kinetic Theory	Kinetic Theory	Kinetic Theory	1050	Kinetic Theory

Table 3 Continued

Thermal Conductivity (w/m-k)	Kinetic Theory	Kinetic Theory	Kinetic Theory	Kinetic Theory	0.0158	Kinetic Theory
Viscosity (kg/m-s)	Kinetic Theory	Kinetic Theory	Kinetic Theory	Kinetic Theory	2.13e-05	Kinetic Theory
Molecular Weight (kg/kgmol)	63.546	34.07	64.06	18.01	159.60	2.01
Standard State Enthalpy (j/kgmol)	0	-2.05e7	-2.9e7	-2.41e+8	0.0158	0
Standard State Entropy (j/kgmol-k)	33.2	205632	20563	188696.4	154719	130579
Reference Temp. (k)	298.15	298.15	298.15	298.15	298.15	298.15
L-J Characteristic Length (Å)	0	2.605	2.605	2.92	-	-

Table 3 Continued

L-J Parameter (K)	0	572.4	572.4	38	-	-
DoF	-	6	18	8	-	-

The reactions in which the defined species participate are to be created in the ANSYS Fluent. Through the solution of the convection-diffusion equation, local mass fraction of each species is predicted by ANSYS FLUENT. After creating the reaction the modifications can be done taking care of the reaction mechanics. The set of reactions, including the reaction type, stoichiometry and rate constants are defined in the mixture materials. The sources and sinks of the chemical species in the gas-phase and the reacting surface are defined through wall surface reactions. The source term is the rate of creation and destruction of the species in the conservation equation. Diffusion to and from the surface along with the chemical kinetics governs rate of adsorption and desorption. The rate of reaction is defined on a volumetric basis [31].

Multiple numbers of reactions can be defined in a reaction drop down dialog box. Every reaction has an individual ID to identify. The reactions can be defined as volumetric, wall surface or particle surface. For the present case the reaction is wall surface type. Total number of reactants and products are defined. For the present case there are four reactants in total, namely, Copper, Humidity, Hydrogen Sulfide and

Sulphur Dioxide and two products namely Copper Sulfate and Hydrogen depending on the equations defined previously. The stoichiometry of the species involved in the reaction, either reactant or product is non-zero. Arrhenius expression is used to compute the forward rate constant with help of inputting pre-exponential factor, temperature exponent, activation energy and universal gas constant.

3.5.2 Cell Zone and Boundary Conditions

Cell zone consists of fluids and solids. ANSYS FLUENT allows solving the problems involving moving parts. The zone type of every zone has to be checked or re-defined if needed before setting up any cell zone or boundary conditions. The flow around the moving part plays interesting role. The flow around the moving parts can be modeled as a steady state problem with respect to moving frame. Moving parts such as rotating blades, moving walls, impellers can be modeled in ANSYS Fluent. In cell zones after the moving reference frame is activated, the equations of the motion are modified to incorporate the additional acceleration terms which occur due to the transformation from the stationary to the moving reference frame. The entire computational domain can be referred as one single moving reference frame. Two formulations are to be addressed when using moving reference frame, namely absolute velocity formulation and relative velocity formulation which appears in momentum equation.

Every zone is associated with the boundary condition. The cell zone and boundary conditions can be copied to other similar zones [31].

All the active equations are solved in fluid zone. Type of fluid material is defined for the fluid zone. An appropriate material property has to be assigned to the fluid zone. For species transportation the material can be specifies as mixture or a fluid. The care should be taken that the fluid zone should not be contiguous. ANSYS Fluent allows setting source or fixed values of scalar quantities. The reaction option can be turned on and the reaction mechanism can be selected for modeling the species transport with reaction [31].

Boundary conditions need to be defined for inlets and outlets, walls, pole and internal face. Different parameters can be defined in the inlet boundary condition.

The gradients are selected for better convergence of the results. Along with the gradients discretization scheme is to be selected in Solution method task page. Second order accuracy is chosen as it gives better result for the species transport reactions. Taylor series expansion is used for second order upwind scheme. Velocity boundary condition can be defined, stating the inlet velocity of the fluid, velocity specification method, reference frame and the initial pressure at the inlet. The inlet temperature of the fluid can be defined. The mole fraction of the gas species selected previously can be defined in the inlet boundary condition depending on the role they play in the reaction mechanics.

For the present study the central shaft, two carousels and eight foils have been given a 2.09 radians/second (20rpm) rotation. Four velocity-inlets at the top (as discussed in previous sections) introduce H_2O (relative humidity) and either H_2S or SO_2 in each simulation at a velocity of 0.5m/s. We would vary the temperature of the whole controlled volume in between 292K (18.89 C) to 298.15 (25 C). 35 parts per millions (ppm) of H_2S or SO_2 is introduced in each simulation. This value is kept constant as per the data from the actual ambient air. The relative humidity is varied from 10% to 60%. The pressure is specified to be pressure-outlet.

The static pressure at the flow outlets and other scalar conditions are defined by the pressure outlet boundary conditions. The flow velocity and pressure at the outlet are not known prior to the simulation so they cannot be specified in the outlet boundary condition dropdown box. The specific loss coefficient and ambient static pressure and temperature at the outlet vent are modeled by the outlet vent boundary conditions. Turbulent parameters can be defined in the inlet and outlet boundary condition dropdown box [31].

Boundary conditions for the pre-defined walls are also to be defined. For rotating boundary condition the rotational axis origin and rotational axis direction are to be defined along with the rotational speed. The thermal parameter has to be defined along with the reaction if the reaction is to be simulated on the particular wall. For the present case the reaction is enabled on the platter in the boundary condition dialogue box and the rotational speed of the platter and the spindle is mentioned along with the thermal parameters of the fluid. The rotational axis origin and the rotational axis direction are also specified. The gravitational force direction is specified on the axis in the operational condition dropdown box along with the operational pressure [31].

3.5.3 Solution Parameters

A well-defined solution technique is employed to obtain a converged solution as there is high degree of coupling between the momentum equations due to high influence of rotational term. Distribution of the rotational speed is set up in the field due to high degree of rotation which introduces large radial pressure gradient, driving the flow in the axial and radial directions [31].

An appropriate scheme has to be selected in solution method dialogue box for better convergence. Quite a few options are available for selecting the scheme for pressure-velocity coupling methods, namely, SIMPLE, SIMPLEC, PISO, and Coupled depending on the properties they offer. For the present study coupled scheme is used. In the coupled scheme all the equations for phase velocity corrections and shared pressure corrections are solved simultaneously. Mass transfer terms and lift forces are incorporated into general matrix by this method. This scheme is most suitable for steady state situations. This scheme is not available if slip velocity is enabled for mixture multiphase model [27]. Under relaxation factors can be varied within the range for better convergence.

Chapter 4

Results and Discussion

4.1 Hydrogen Sulfide Analysis

A total of 54 simulations were carried out to study the effect of H_2S. Relative humidity was specified in the steps of 10%. The relative humidity was taken to be 10%, 20%, 30%, 40%, 50% and 60% for individual simulation at a fix temperature (Case 4.1.1 to Case 4.1.9) For the next part of analysis temperature was increased insteps of 1K keeping the relative humidity constant. Temperatures that were used are 292K, 293K, 294K, 295K, 296K, 297K, 298K, 299K and 300K Case 4.1.10 to Case 4.1.15)

Surface deposition rate would be studied. The Surface deposition is the product of reaction ($CuSO_4$). ANSYS Fluent gives the results in ($\frac{kg}{m^2.s^1}$). This would be converted to Å/month, which is the actual unit of corrosion measurement in IT equipment

4.1.1 Case at 300K varying the relative humidity

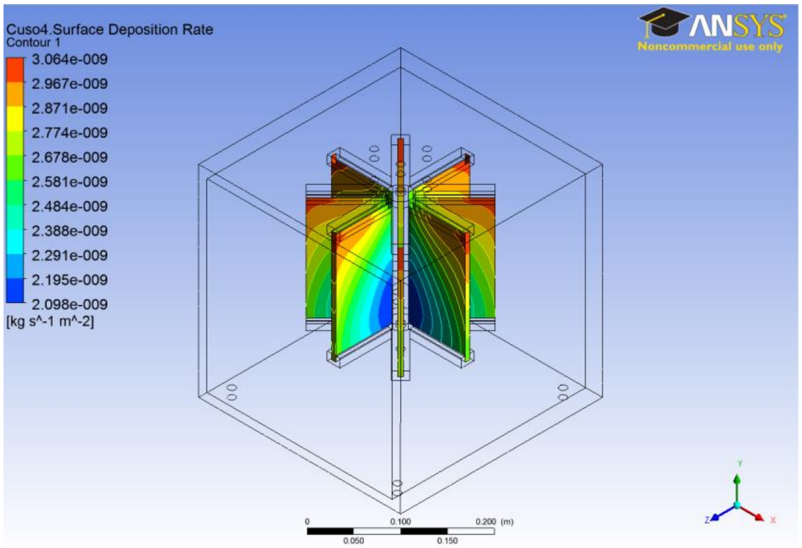

Figure 22 Corrosion at 300K and 20%RH

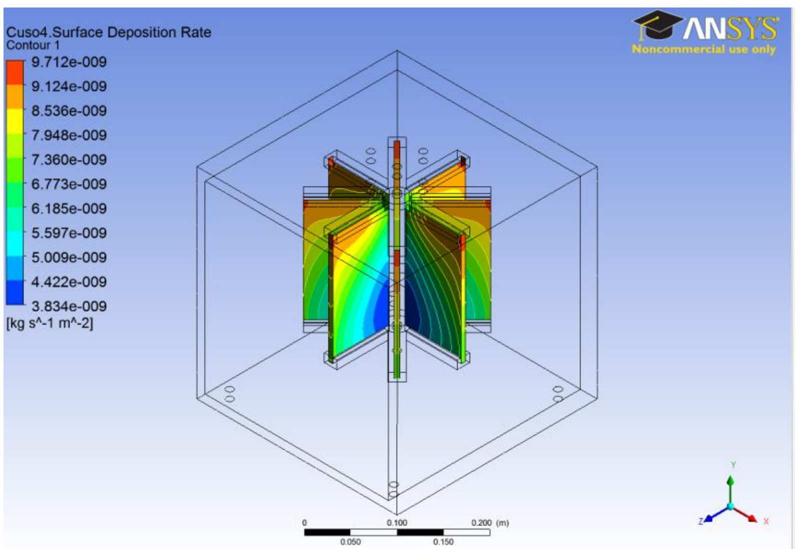

Figure 23 Corrosion at 300K and 40%RH

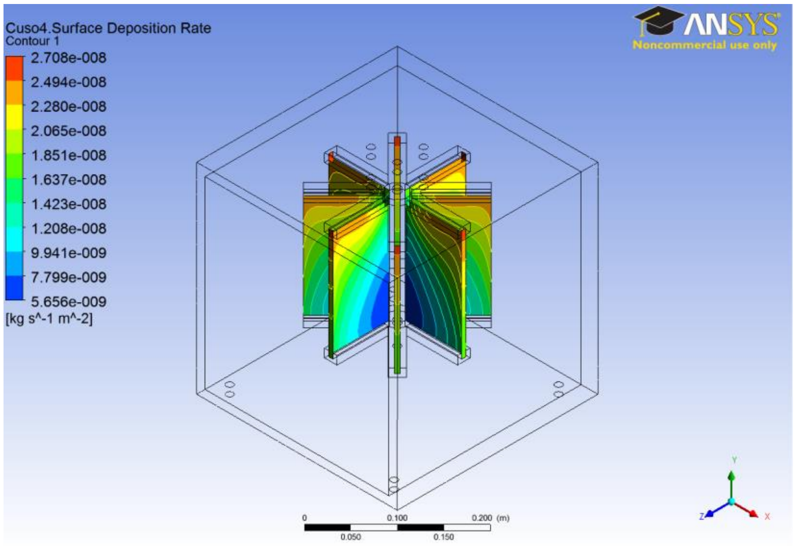

Figure 24 Corrosion at 300K and 60%RH

A graph can be plotted to study the effects of H2S.

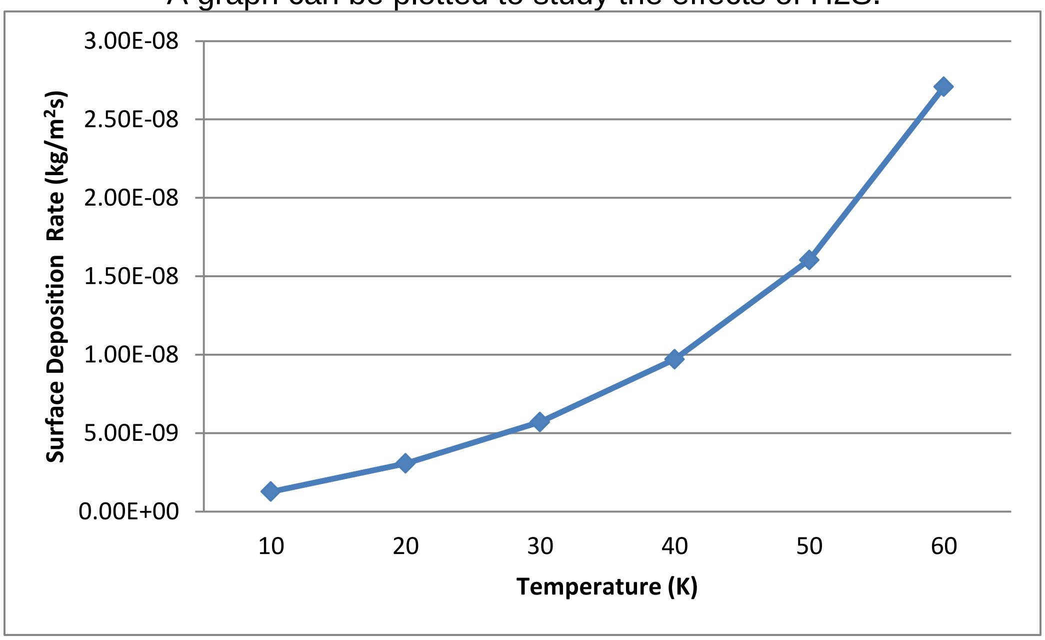

Figure 25 Relative humidity v/s Surface Deposition rate (kg/m2s) at 300K

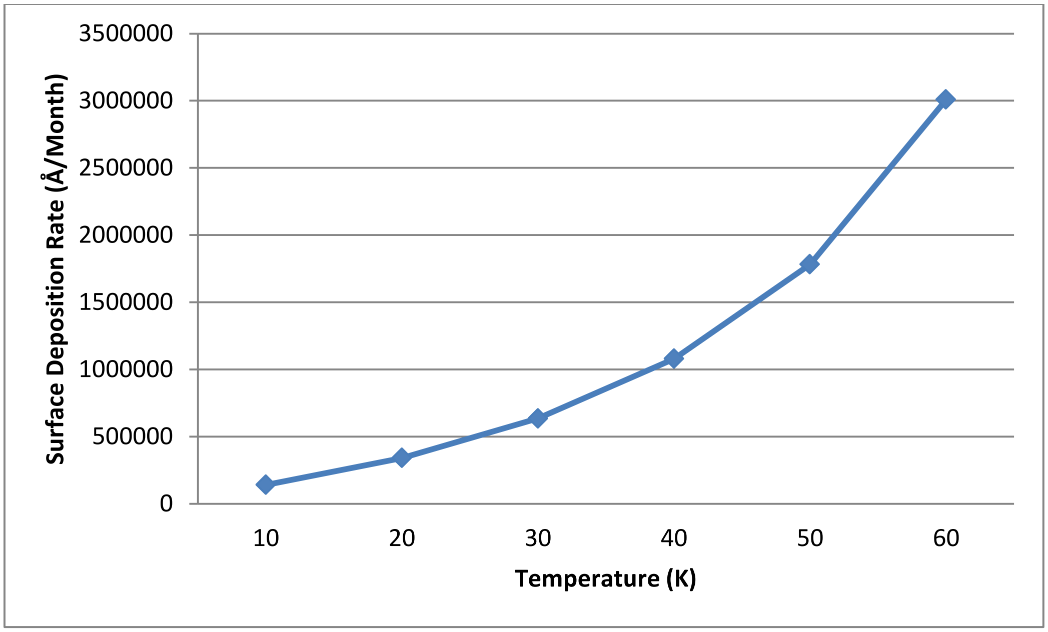

Figure 26 Relative humidity v/s Surface Deposition rate (Å/month) at 300K

Table 4 Surface Deposition Rate at varying RH (at 300K)

Relative Humidity (%)	Surface Deposition Rate (kg/m^{2}s)x10-^{9}	Surface Deposition Rate (Å/month)x10^3
10	1.261	140.111
20	3.064	340.444
30	5.707	634.111
40	9.712	1079.111
50	16.04	1782.222
60	2.708	3008.888

In this case it is obviously clear that the corrosion increases as the humidity increases at a given temperature.

4.1.2 Case at 299K and varying Relative Humidity

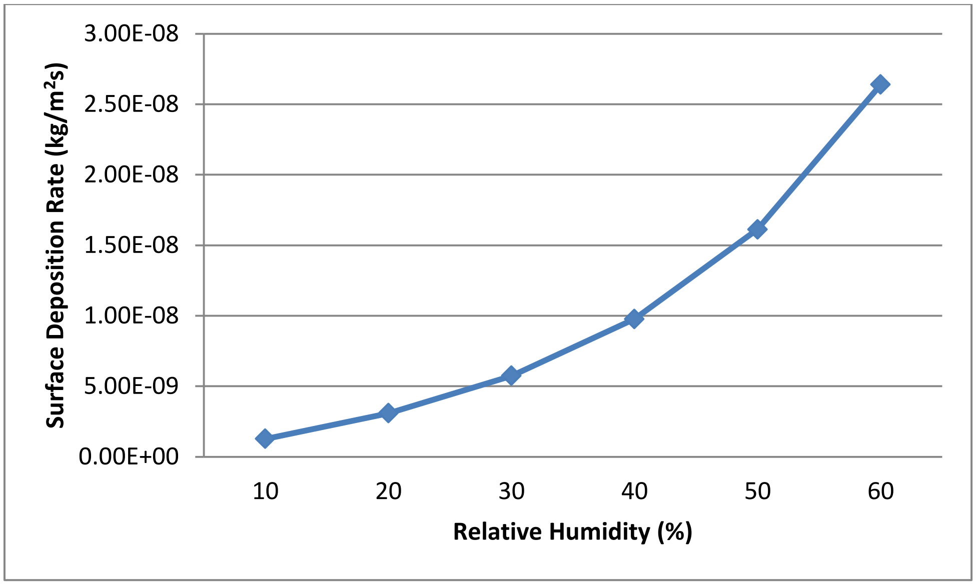

Figure 27 Relative humidity v/s Surface Deposition rate (kg/m2s) at 299K

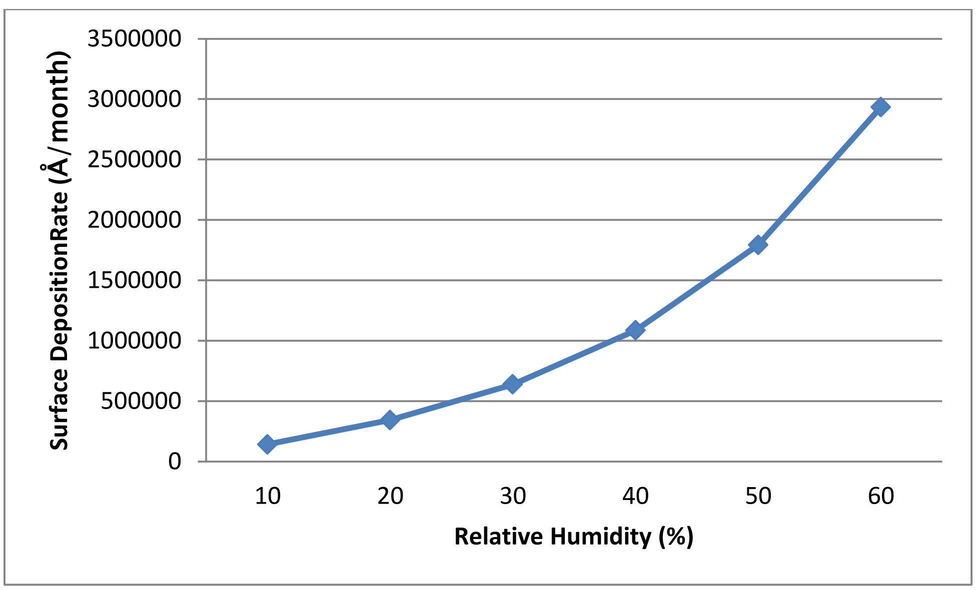

Figure 28 Relative humidity v/s Surface Deposition rate (Å/month) at 299K

Table 5 Surface Deposition Rate at varying RH (at 299K)

Relative Humidity (%)	Surface Deposition Rate (kg/m^{2}s)x10-^{9}	Surface Deposition Rate (Å/month)x10^3
10	1.267	140.778
20	3.079	342.111
30	5.736	637.333
40	9.759	1084.333
50	16.12	1791.111
60	26.39	2932.222

As seen the plot in this case resembles to that of 300K

4.1.3 Case at 298K and varying Relative Humidity

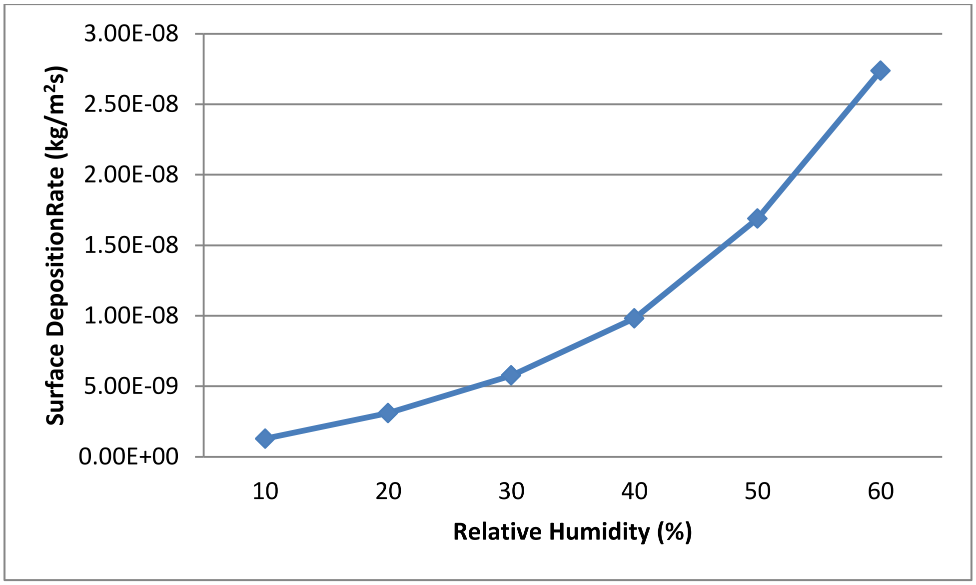

Figure 29 Relative humidity v/s Surface Deposition rate (kg/m2s) at 298K

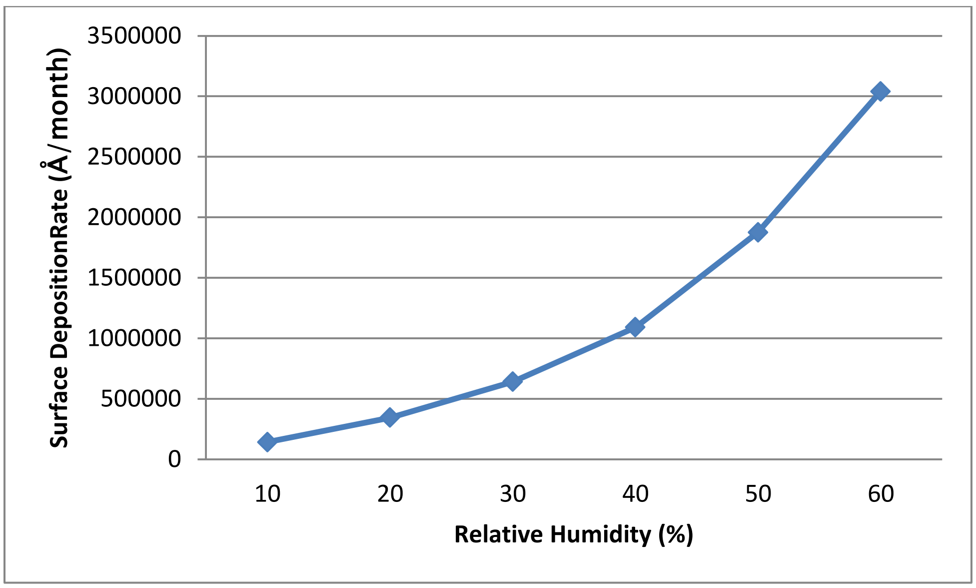

Figure 30 Relative humidity v/s Surface Deposition rate (Å/month) at 298K

Table 6 Surface Deposition Rate at varying RH (at 298K)

Relative Humidity (%)	Surface Deposition Rate $(kg/m^2s)x10^{-9}$	Surface Deposition Rate $(Å/month)x10^3$
10	1.274	141.556
20	3.095	343.889
30	5.764	640.444
40	9.808	1089.778
50	16.88	187.556
60	27.36	304.000

In this case at 298K the plot shows the same behavior indicating the ride in corrosion rate

4.1.4 Case at 297K and varying Relative Humidity

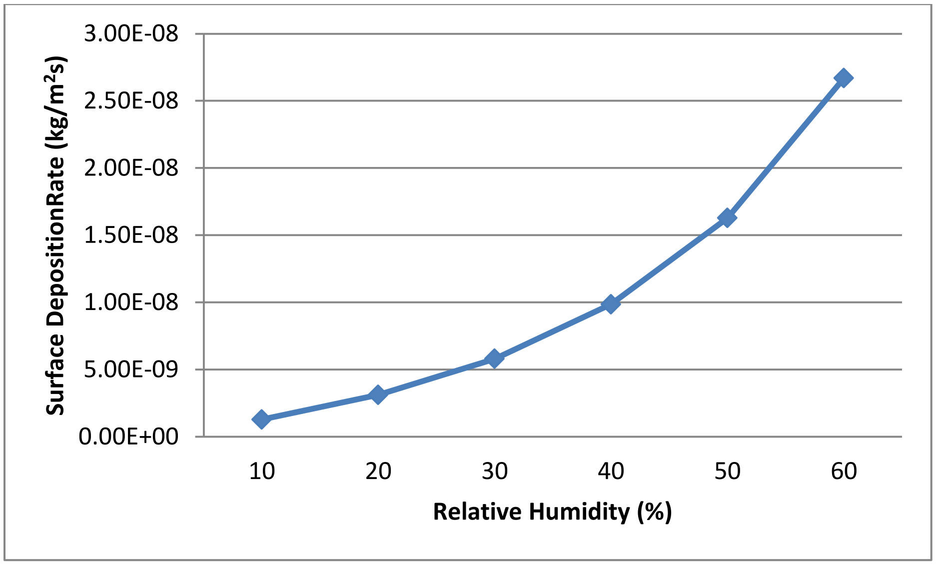

Figure 31 Relative humidity v/s Surface Deposition rate (kg/m2s) at 297K

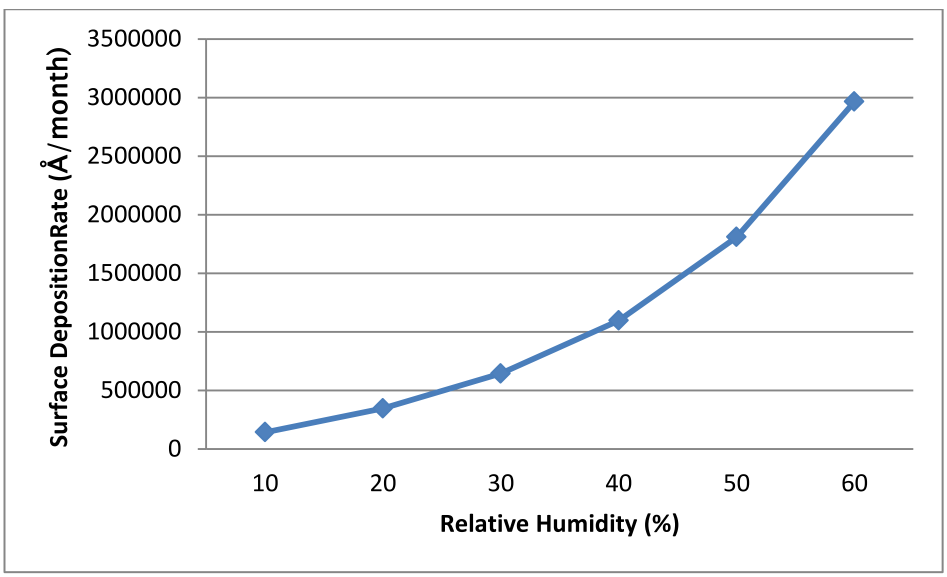

Figure 32 Relative humidity v/s Surface Deposition rate (Å/month) at 297K

Table 7Surface Deposition Rate at varying RH (at 297K)

Relative Humidity (%)	Surface Deposition Rate $(kg/m^2s)x10^{-9}$	Surface Deposition Rate $(\text{Å}/month)x10^3$
10	1.280	142.222
20	3.110	345.556
30	5.794	643.778
40	9.857	1095.222
50	16.27	180.778
60	26.68	296.444

The same behavior is seen in this case (at 297K and varying relative humidity levels as well)

4.1.5 Case at 296K and varying Relative Humidity

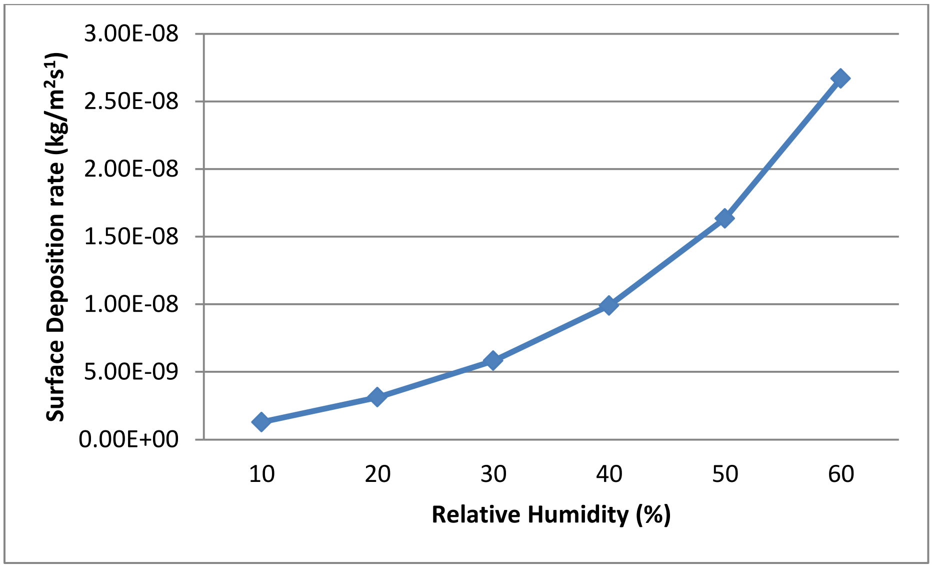

Figure 33 Relative humidity v/s Surface Deposition rate (kg/m2s) at 296K

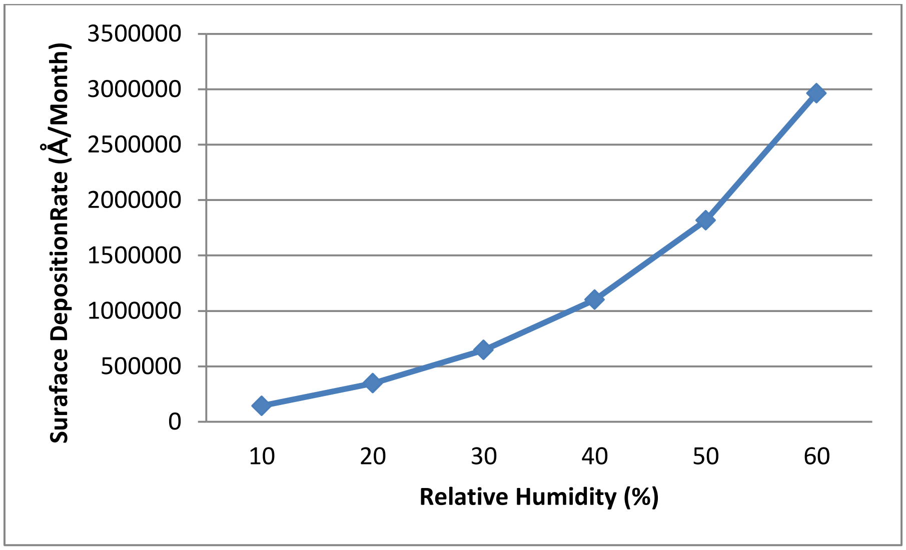

Figure 34 Relative humidity v/s Surface Deposition rate (Å/month) at 296K

Table 8 Surface Deposition Rate at varying RH (at 296K)

Relative Humidity (%)	Surface Deposition Rate $(kg/m^2s)x10^{-9}$	Surface Deposition Rate (Å/month)$x10^3$
10	1.287	143.000
20	3.126	347.333
30	5.823	647.000
40	9.907	1100.778
50	16.35	1816.667
60	26.68	2964.444

Same trend is followed by the corrosion rate in this case as well.

4.1.6 Case at 295K and varying Relative Humidity

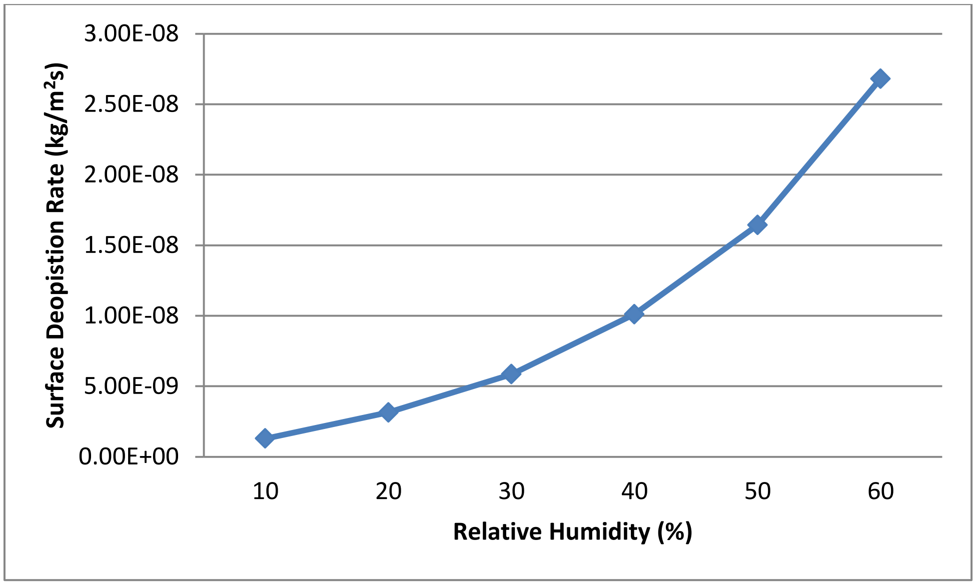

Figure 35 Relative humidity v/s Surface Deposition rate (kg/m2s) at 295K

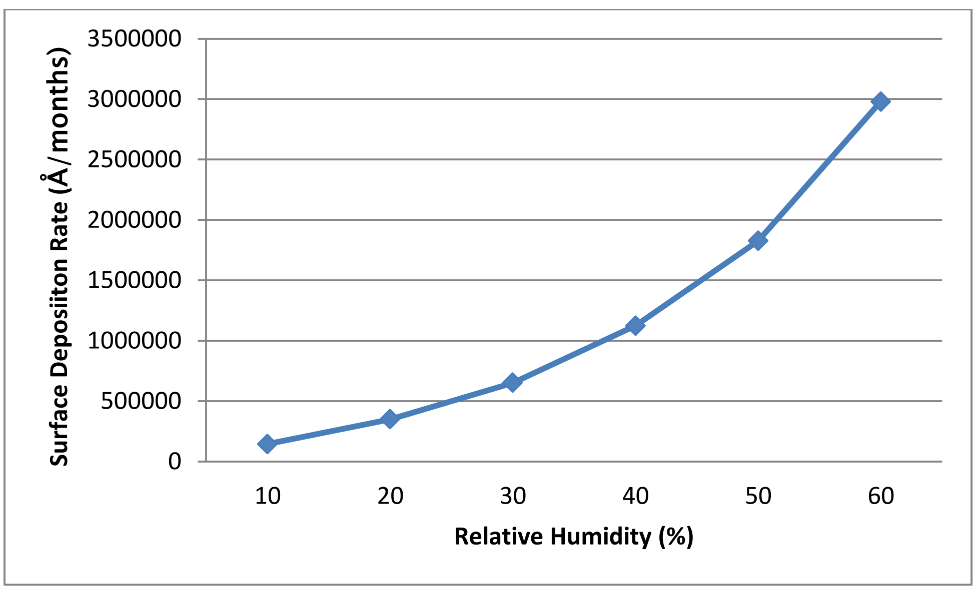

Figure 36 Relative humidity v/s Surface Deposition rate (Å/month) at 295K

Table 9 Surface Deposition Rate at varying RH (at 295K)

Relative Humidity (%)	Surface Deposition Rate $(kg/m^2s)x10^{-9}$	Surface Deposition Rate (Å/month)$x10^3$
10	1.293	143.667
20	3.142	349.111
30	5.852	650.222
40	10.111	1123.333
50	16.43	1825.556
60	26.81	2978.889

The present case has also shown the same trend

4.1.7 Case at 294K and varying Relative Humidity

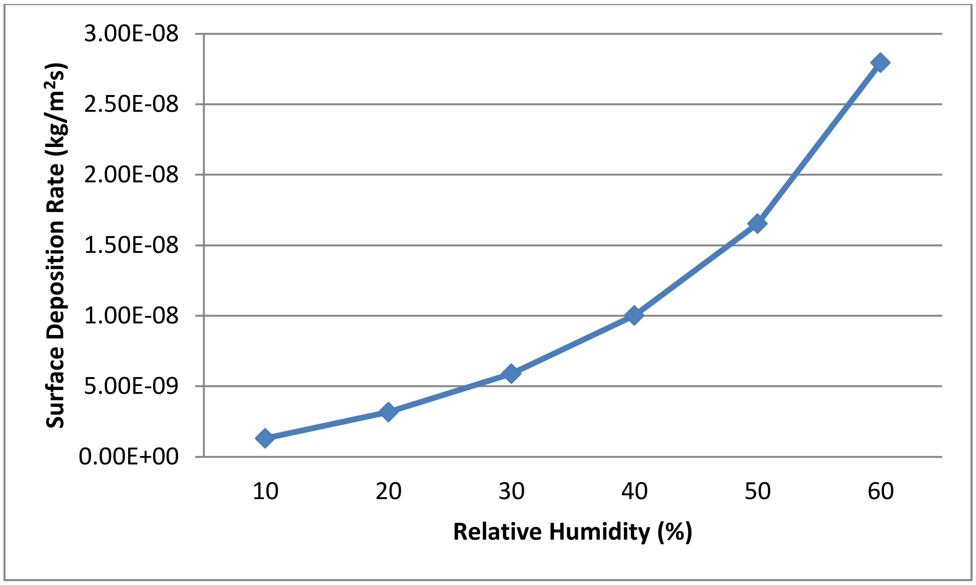

Figure 37 Relative humidity v/s Surface Deposition rate (kg/m2s) at 294K

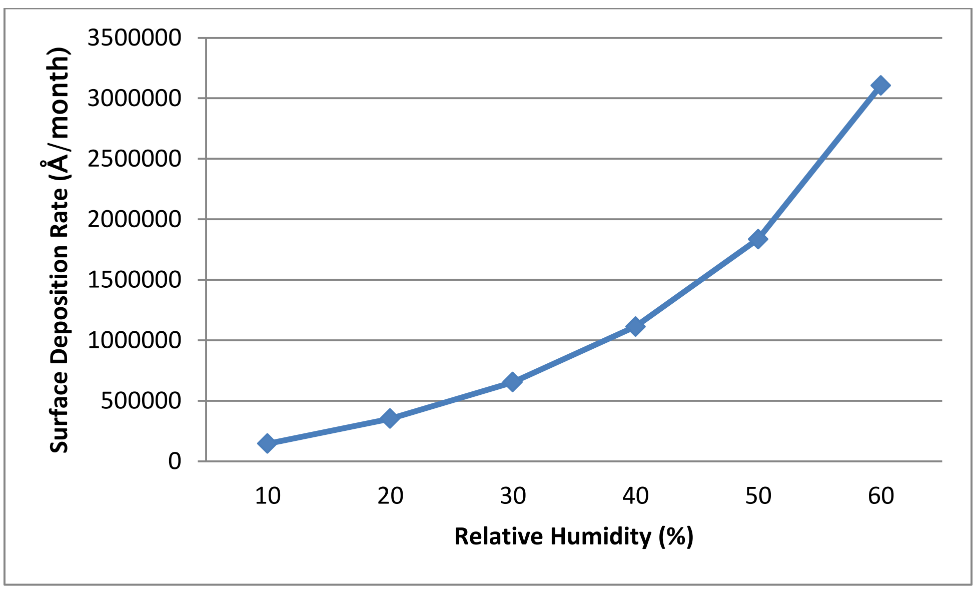

Figure 38 Relative humidity v/s Surface Deposition rate (Å/month) at 294K

Table 10 Surface Deposition Rate at varying RH (at 294K)

Relative Humidity (%)	Surface Deposition Rate (kg/m^{2}s)x10-^{9}	Surface Deposition Rate (Å/month)x10^3
10	1.30	144.444
20	3.158	350.889
30	5.882	653.556
40	10.001	1112.222
50	16.52	1835.556
60	27.94	3104.444

Same trend has been observed here as well.

4.1.8 Case at 293K and varying Relative Humidity

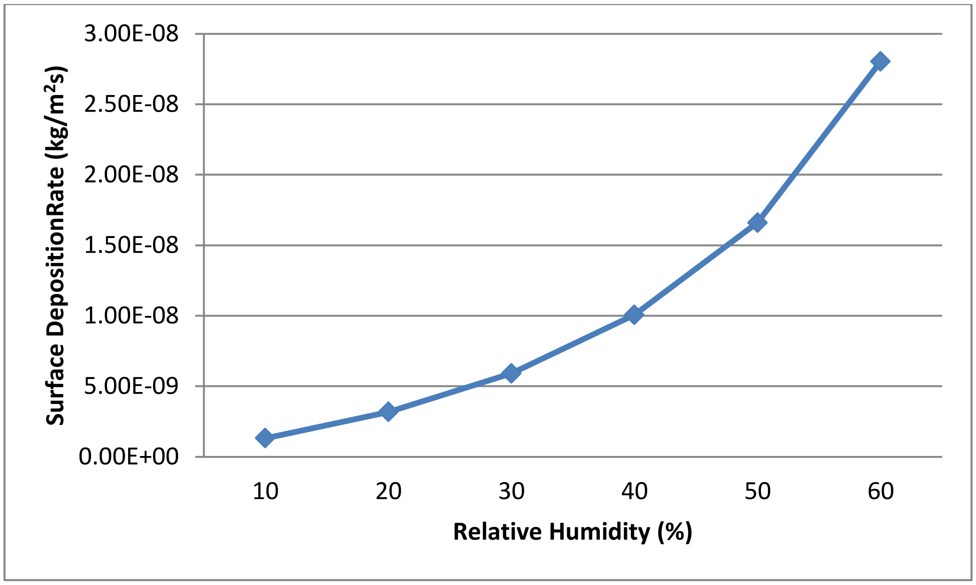

Figure 39 Relative humidity v/s Surface Deposition rate (kg/m2s) at 293K

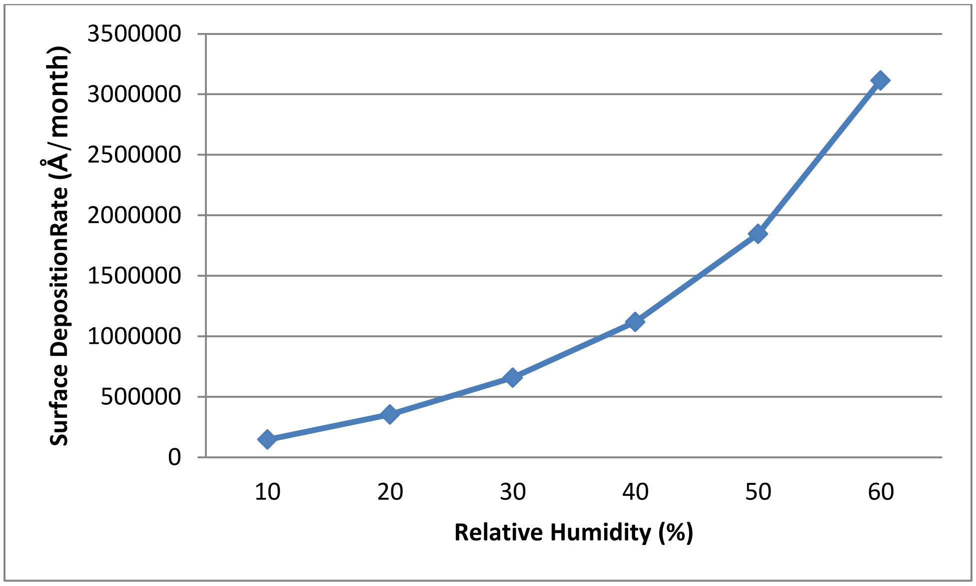

Figure 40 Relative humidity v/s Surface Deposition rate (Å/month) at 293K

Table 11 Surface Deposition Rate at varying RH (at 293K)

Relative Humidity (%)	Surface Deposition Rate $(kg/m^2s)x10^{-9}$	Surface Deposition Rate $(Å/month)x10^3$
10	1.307	145.222
20	3.174	352.667
30	5.911	656.778
40	10.006	1117.778
50	16.60	1844.444
60	28.03	3114.444

It is again seen that the relative humidity is playing a major role in corrosion rate.

4.1.9 Case at 292K and varying Relative Humidity

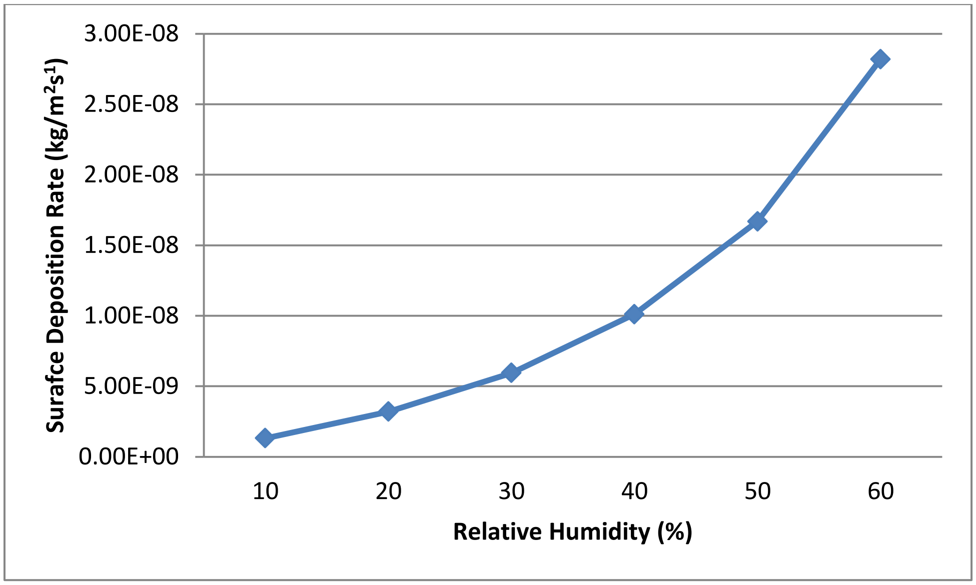

Figure 41 Relative humidity v/s Surface Deposition rate (kg/m2s) at 292K

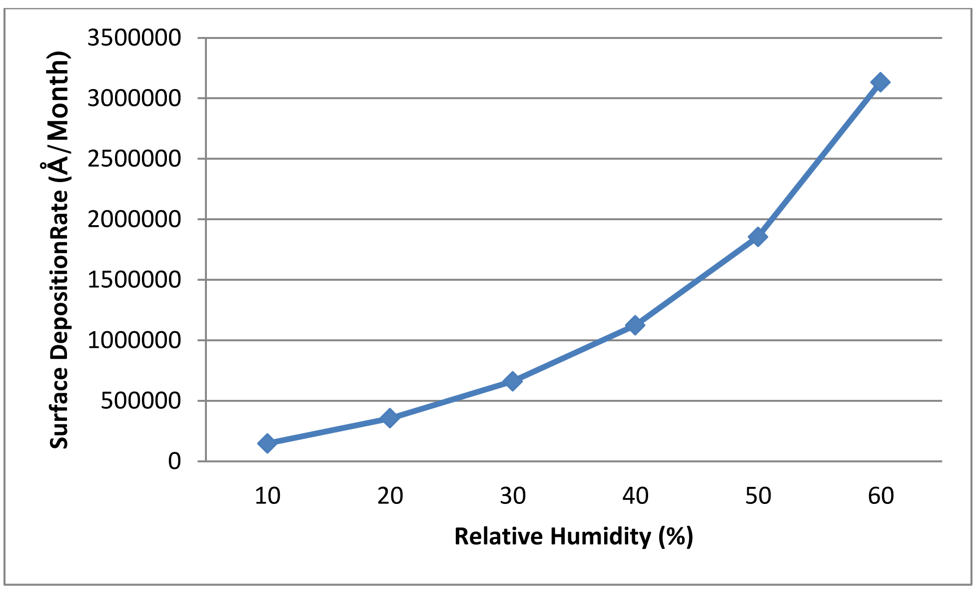

Figure 42 Relative humidity v/s Surface Deposition rate (Å/month) at 292K

Table 12 Surface Deposition Rate at varying RH (at 292K)

Relative Humidity (%)	Surface Deposition Rate (kg/m^{2}s)x10-^{9}	Surface Deposition Rate (Å/month)x10^3
10	1.313	145.889
20	3.190	354.444
30	5.942	660.222
40	10.011	1123.333
50	16.68	1853.333
60	28.19	3132.222

This would be the last set of simulations in this category of varying the relative humidity range and keeping the temperature constant. As seen throughout the plots the corrosion has increased in steps when we increase the humidity levels from 10% to 60%

4.1.10 Case at 60% Relative humidity varying the temperature

The test in this section we would simulate the test setup for varying temperature while keeping the relative humidity constant

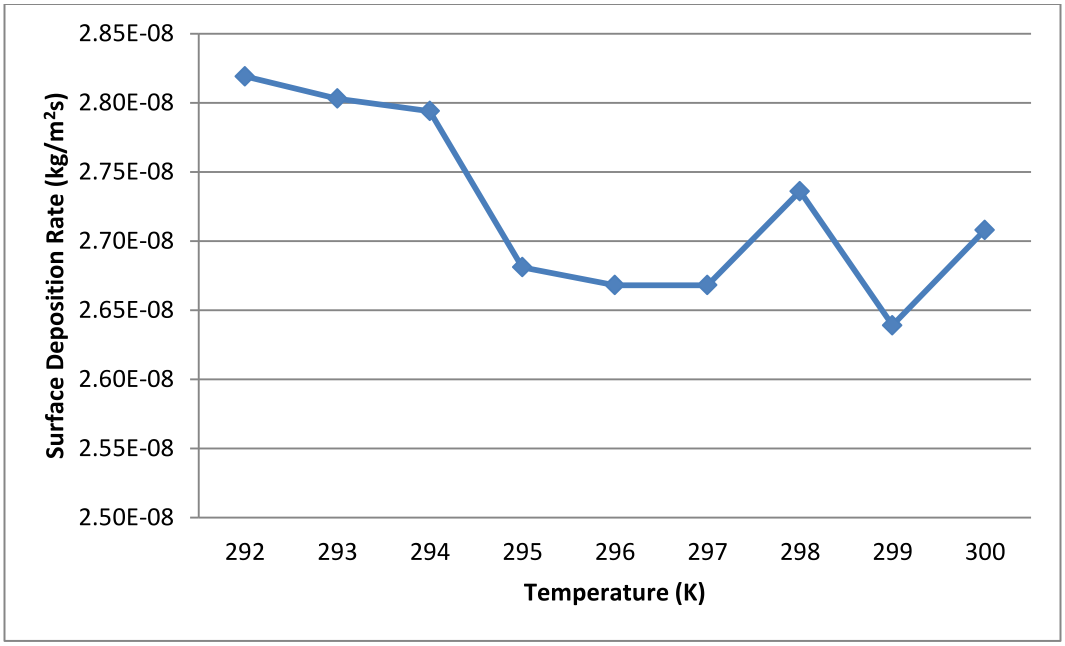

Figure 43 Temperature v/s Surface Deposition rate (kg/m2s) at 60% RH

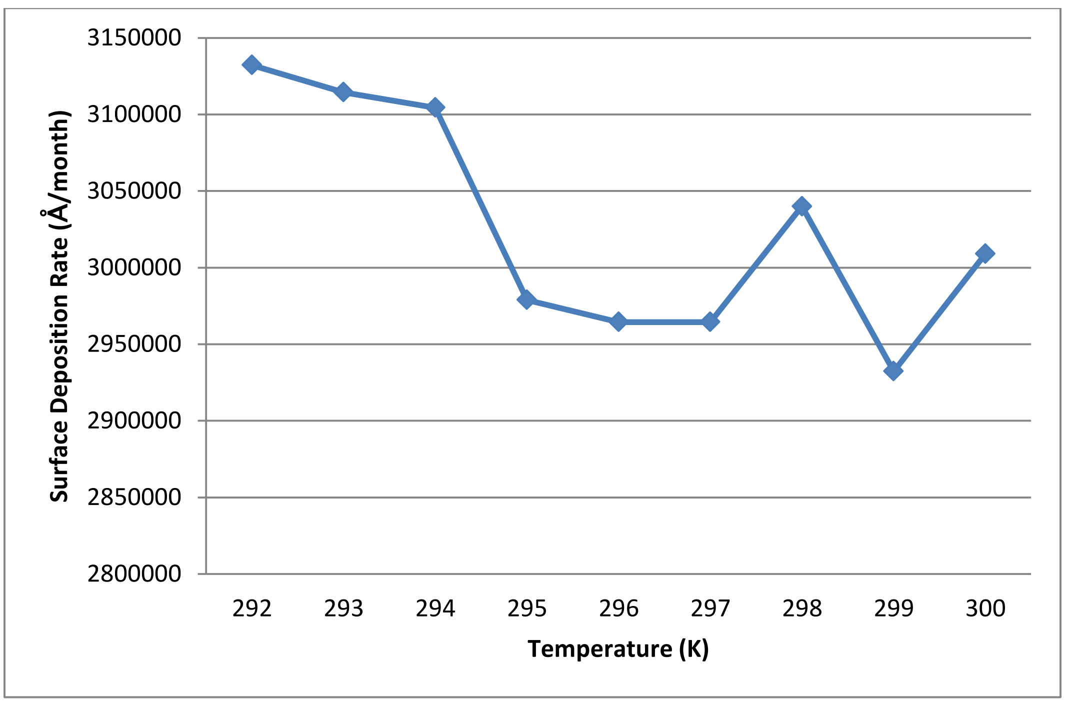

Figure 44 Temperature v/s Surface Deposition rate (Å/month) at 60% RH

Table 13 Surface Deposition Rate at varying Temperature (at 60%RH)

Temperature (K)	Surface Deposition Rate $(kg/m^2s) \times 10^{-8}$	Surface Deposition Rate (Å/month)$\times 10^{3}$
292	2.819	3132.222
293	2.803	3114.444
294	2.794	3104.444
295	2.618	2978.889
296	2.668	2964.444
297	2.668	2964.444
298	2.736	3040.000
299	2.639	2932.222
300	2.708	3008.889

As seen from the graph the corrosion rate has shown a shift from the regular trend as we observed in the previous simulations. The corrosion rate was at its peak at 292K while it abruptly increased at 298K and 300K.

4.1.11 Case at 50%RH varying the temperature

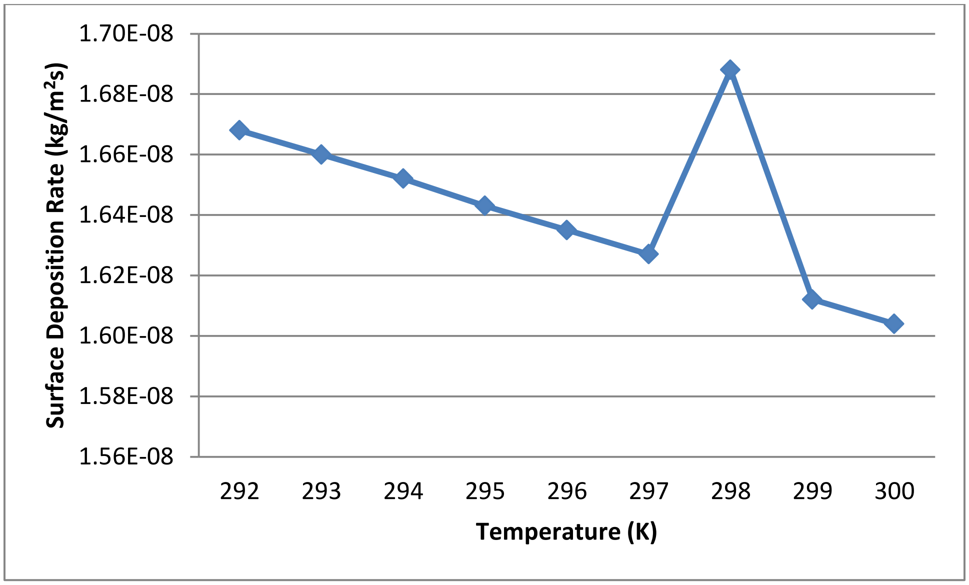

Figure 45 Temperature v/s Surface Deposition rate (kg/m2s) at 50% RH

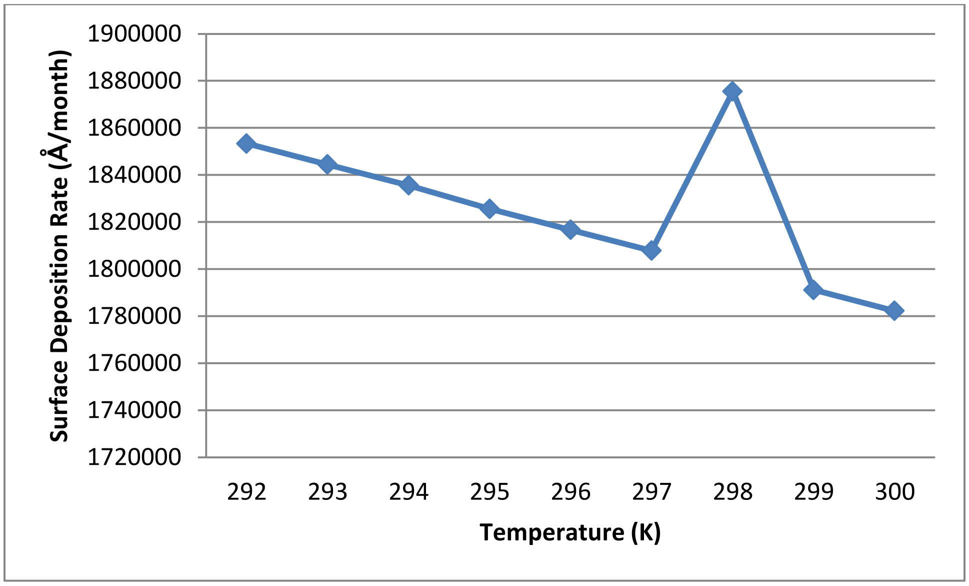

Figure 46 Temperature v/s Surface Deposition rate (Å/month) at 50% RH

Table 14 Surface Deposition Rate at varying Temperature (at 50%RH)

Temperature (K)	Surface Deposition Rate $(kg/m^2s)x10^{-8}$	Surface Deposition Rate $(Å/month)x10^3$
292	1.668	1853.333
293	1.660	1844.444
294	1.652	1835.556
295	1.643	1825.556
296	1.635	1816.667
297	1.627	1807.778
298	1.688	1875.556
299	1.612	1791.111
300	1.604	1782.222

An unconfirmed behavior has been observed in this case as well. At 298K the corrosion rate has peaked up. While the rest of the slope has a smooth gradient.

4.1.12 Case at 40% Relative Humidity varying the temperature

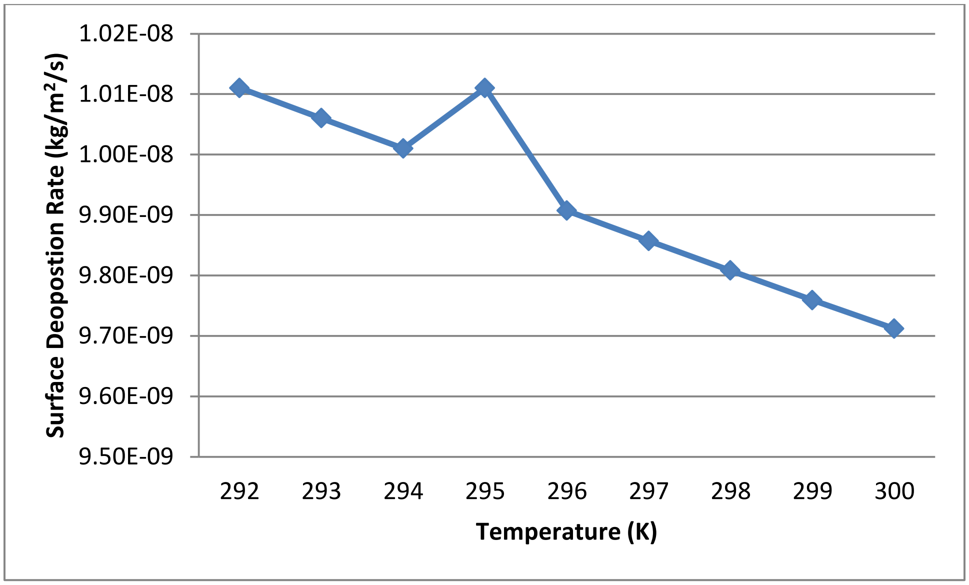

Figure 47Temperature v/s Surface Deposition rate (kg/m2s) at 40% RH

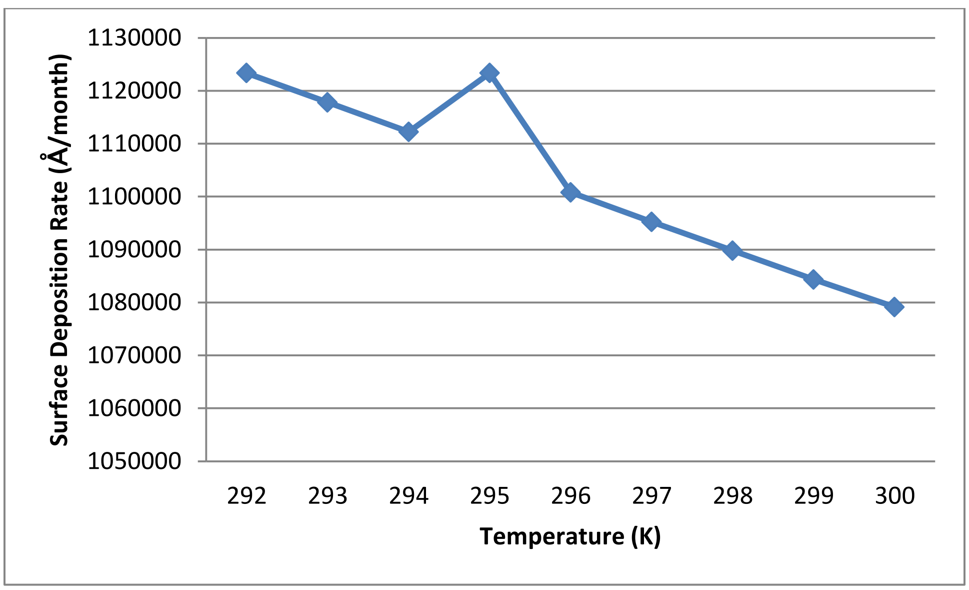

Figure 48 Temperature v/s Surface Deposition rate (Å/month) at 40% RH

Table 15 Surface Deposition Rate at varying Temperature (at 40%RH)

Temperature (K)	Surface Deposition Rate $(kg/m^2s)x10^{-9}$	Surface Deposition Rate $(Å/month)x10^3$
292	10.11	1123.333
293	10.06	1117.778
294	10.01	1112.222
295	10.11	1123.333
296	9.907	1100.778
297	9.857	1095.222
298	9.808	1089.778
299	9.759	1084.333
300	9.712	1079.111

In this case as well the corrosion rate went up at 295K. Thus, not showing a behavior that we observed in the previous cases.

4.1.13 Case at 30% Relative Humidity varying the Temperature

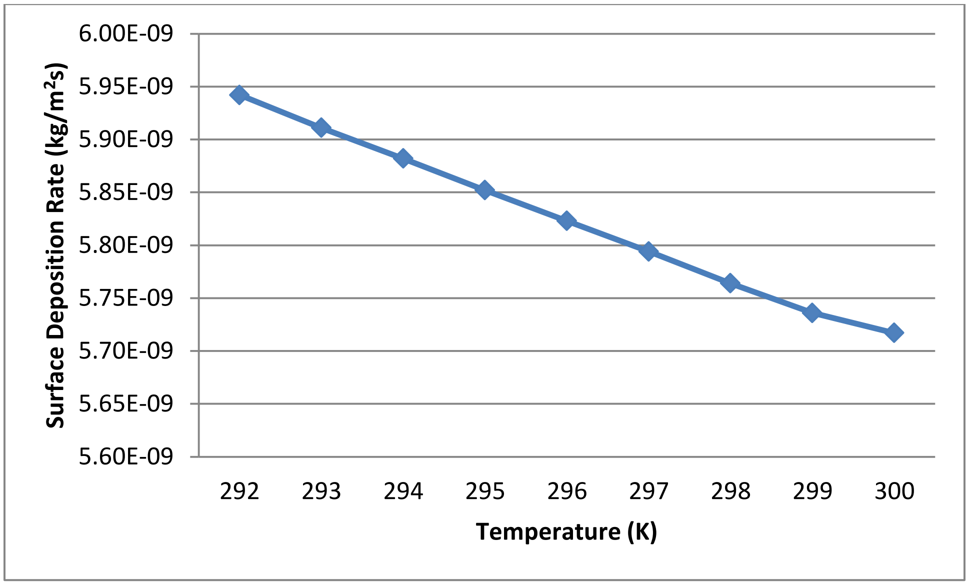

Figure 49 Temperature v/s Surface Deposition rate (kg/m2s) at 30% RH

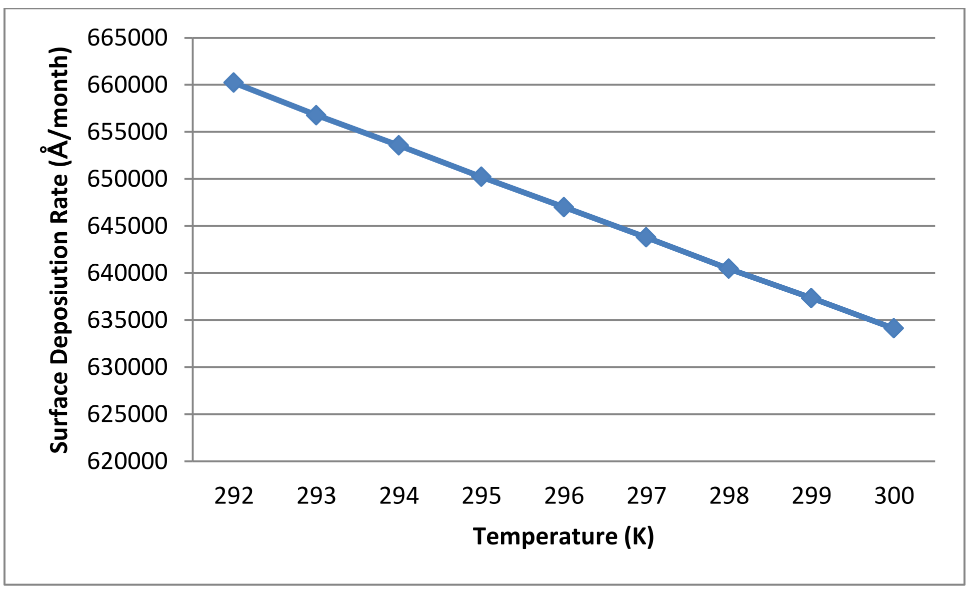

Figure 50 Temperature v/s Surface Deposition rate (Å/month) at 30% RH

Table 16 Surface Deposition Rate at varying Temperature (at 30%RH)

Temperature (K)	Surface Deposition Rate (kg/m^{2}s)x10^{-9}	Surface Deposition Rate (Å/month)x10^3
292	5.942	6602.222
293	5.911	6567.778
294	5.882	6535.556
295	5.852	6502.222
296	5.823	6470.000
297	5.794	6437.778
298	5.764	6404.444
299	5.736	6373.333
300	5.707	6341.111

Unlike the earlier cases this case has shown a smooth slope thus signifying that the corrosion rate is decreasing at we are increasing the temperature.

4.1.14 Case at 20% Relative Humidity and varying the Temperature

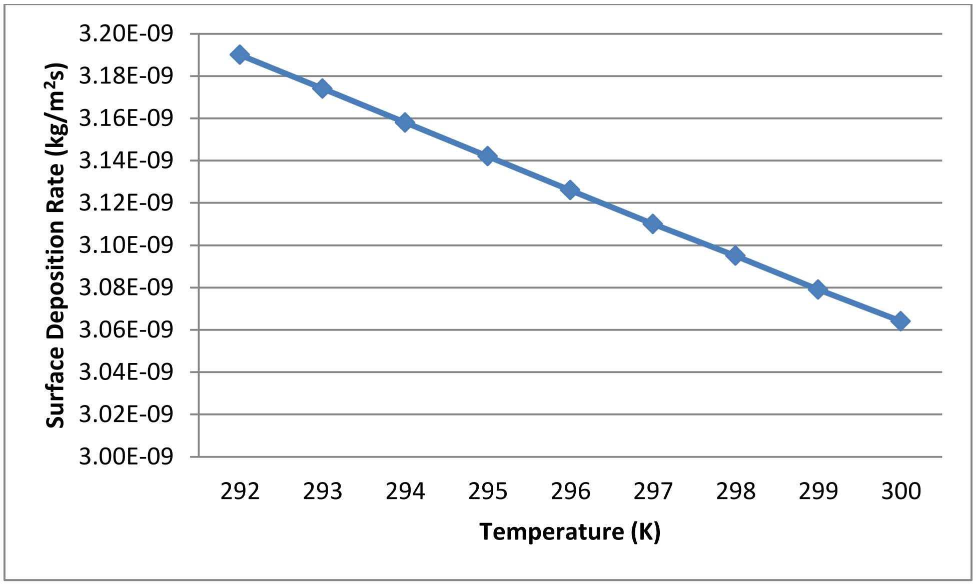

Figure 51 Temperature v/s Surface Deposition rate (kg/m2s) at 20% RH

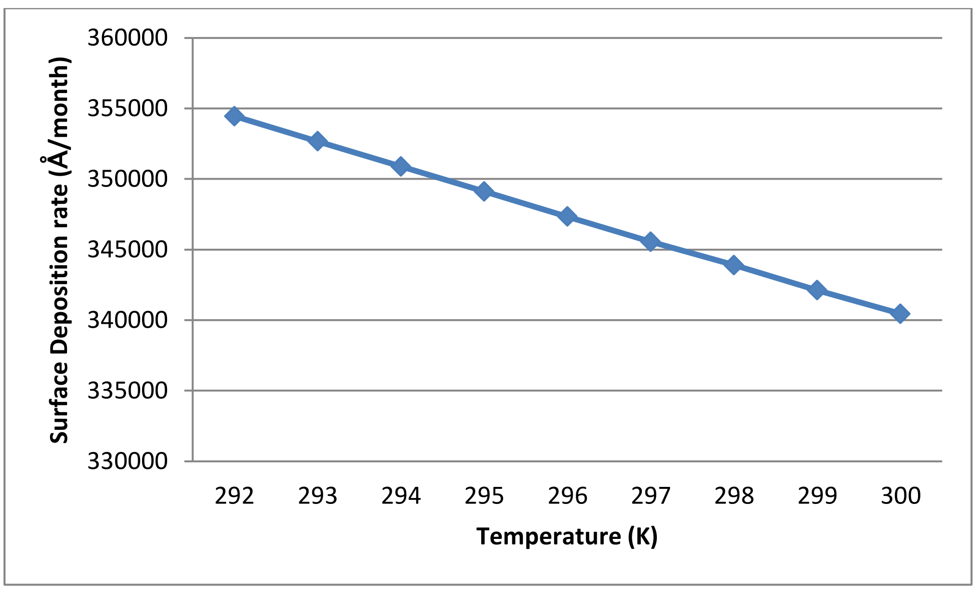

Figure 52 Temperature v/s Surface Deposition rate (Å/month) at 20% RH

Table 17 Surface Deposition Rate at varying Temperature (at 20%RH)

Temperature (K)	Surface Deposition Rate $(kg/m^2s)x10^{-9}$	Surface Deposition Rate (Å/month)$x10^3$
292	3.190	3544.444
293	3.174	3526.667
294	3.158	3508.889
295	3.142	3491.111
296	3.126	3473.333
297	3.11	3455.556
298	3.095	3438.889
299	3.079	3421.111
300	3.064	3404.444

Corrosion rate has shown the same smooth slope behavior in this case as well.

4.1.15 Case at 10% Relative Humidity varying the Temperature

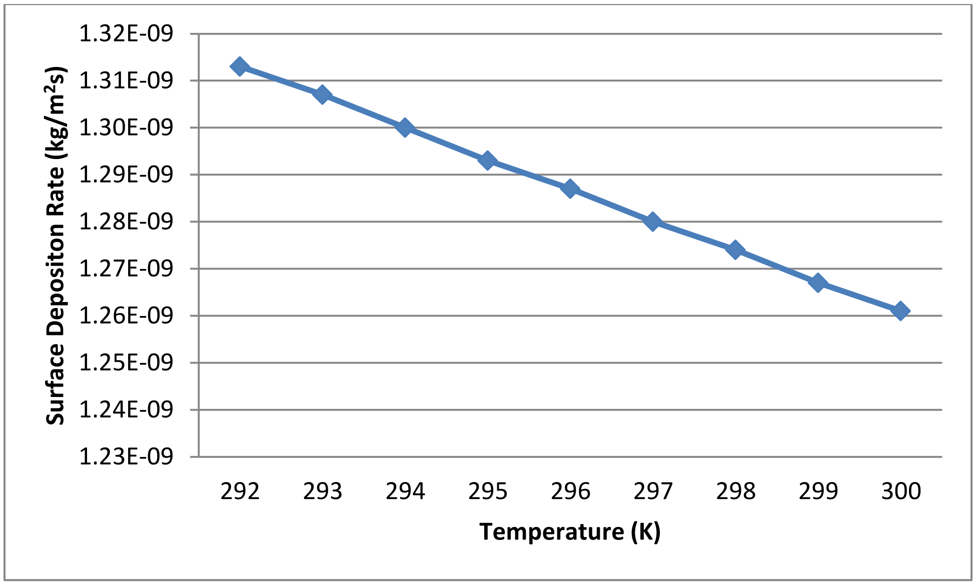

Figure 53 Temperature v/s Surface Deposition rate (kg/m2s) at 10% RH

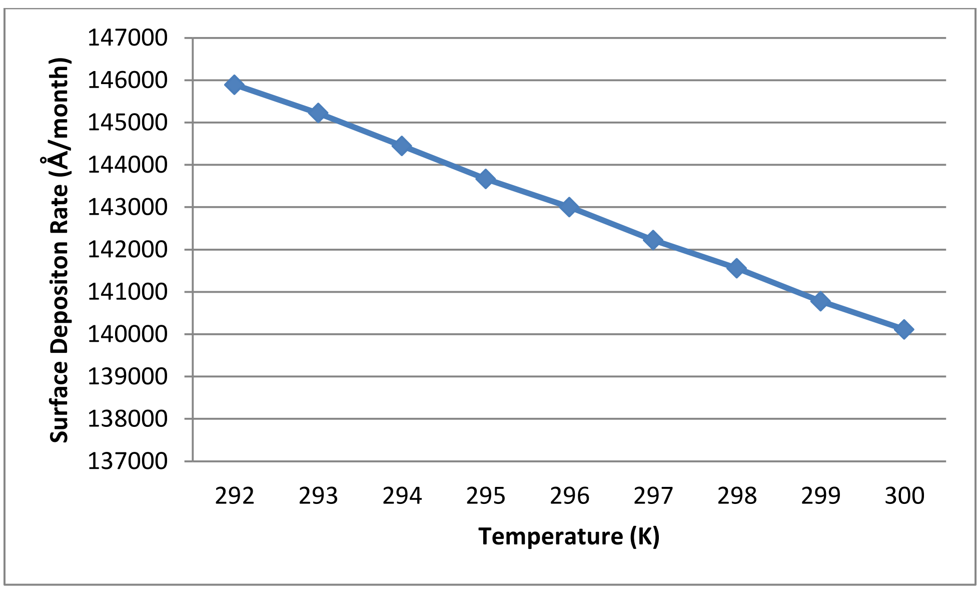

Figure 54 Temperature v/s Surface Deposition rate (Å/month) at 10% RH

Table 18 Surface Deposition Rate at varying Temperature (at 10%RH)

Temperature (K)	Surface Deposition Rate $(kg/m^2s)x10^{-9}$	Surface Deposition Rate $(Å/month)x10^3$
292	1.313	1458.889
293	1.307	1452.222
294	1.300	1444.444
295	1.293	1436.667
296	1.287	1430.000
297	1.280	1422.222
298	1.274	1415.556
299	1.267	1407.778
300	1.261	1401.111

The slope in this case has the same nature. This would be the last sets of simulations in this case of varying the temperature range while keeping the Relative humidity constant.

4.2 Sulfur Dioxide Analysis

A total of 54 simulations were carried out to study the effect of SO_2 as well. Relative humidity was increased in the steps of 10%. The relative humidity was taken to be 10%, 20%, 30%, 40%, 50% and 60% for individual simulation at a fix temperature (Case 4.2.1 to Case 4.2.9) For the next part of analysis temperature was increased insteps of 1K keeping the relative humidity constant. Temperatures that were used are 292K, 293K, 294K, 295K, 296K, 297K, 298K, 299K and 300K (4.2.10 to 4.2.15)

4.2.1 Case at 300K varying the relative humidity

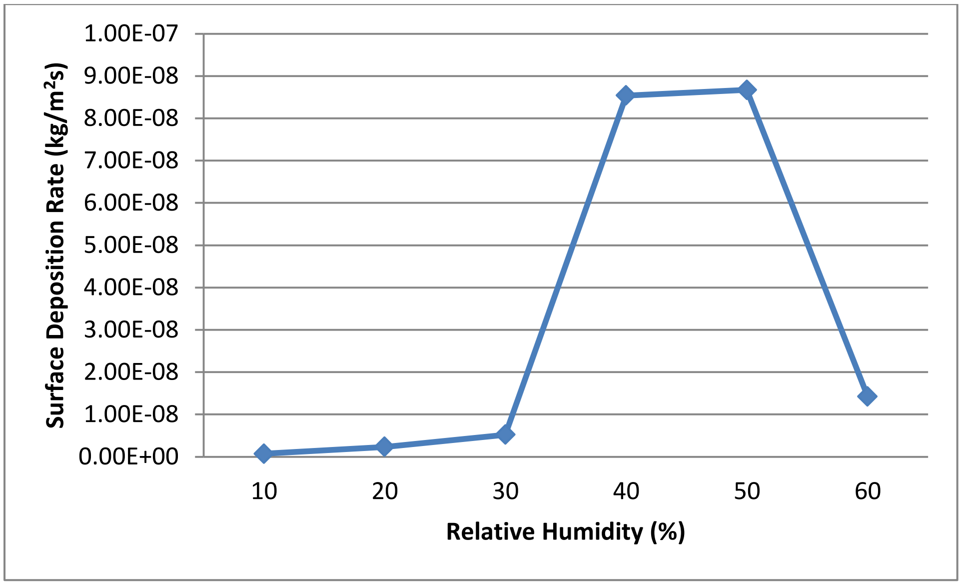

Figure 55 Relative humidity v/s Surface Deposition rate (kg/m2s) at 300K

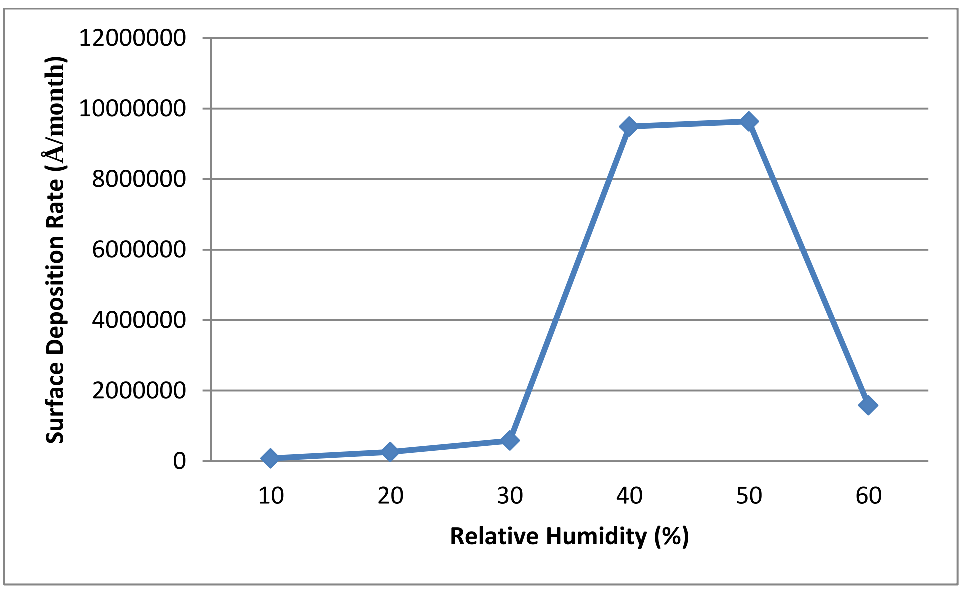

Figure 56 Relative humidity v/s Surface Deposition rate (Å/month) at 300K

Table 19 Surface Deposition Rate at varying RH (at 300K)

Relative Humidity (%)	Surface Deposition Rate (kg/m^{2}s)x10^{-9}	Surface Deposition Rate (Å/month)x10^3
10	0.6946	771.778
20	2.315	257.222
30	5.209	578.778
40	85.38	9486.667
50	86.71	9634.444
60	14.25	1583.333

Unlike the effect of Hydrogens sulfide at the given conditions Sulfur Dioxide has shown a different behavior. The corrosion peaked up at 40% and 50% relative humidity at the given 300K temperature.

4.2.2 Case at 299K varying the relative humidity

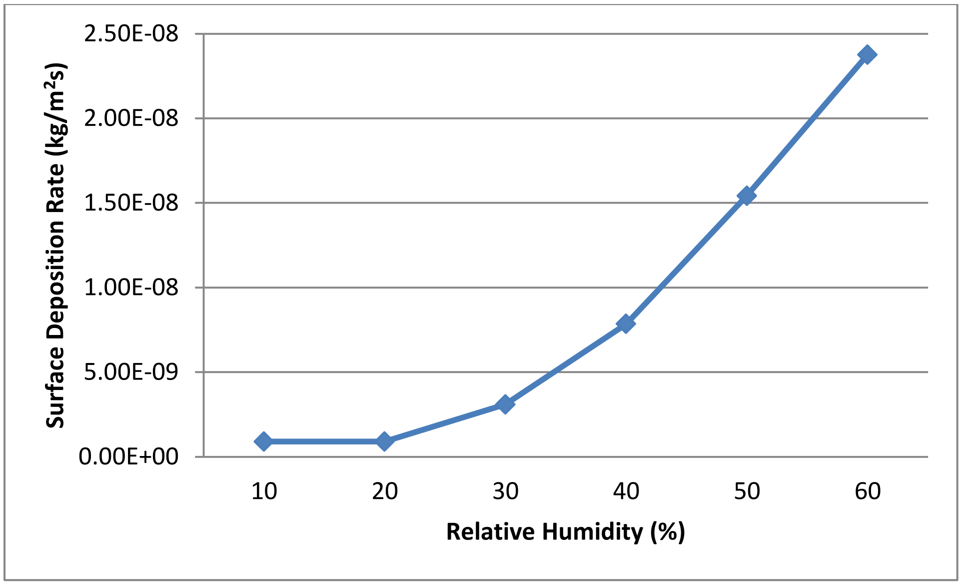

Figure 57 Relative humidity v/s Surface Deposition rate (kg/m2s) at 299K

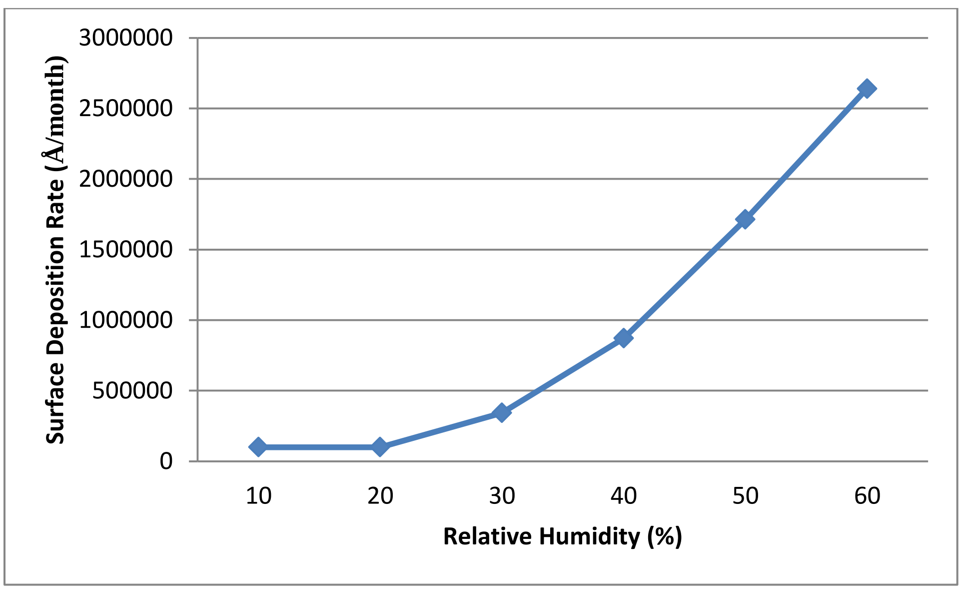

Figure 58 Relative humidity v/s Surface Deposition rate (Å/month) at 299K

Table 20 Surface Deposition Rate at varying RH (at 299K)

Relative Humidity (%)	Surface Deposition Rate (kg/m^2s)x10^{-9}	Surface Deposition Rate (Å/month)x10^3
10	0.8982	99.800
20	0.8982	99.800
30	3.083	342.556
40	7.843	871.444
50	1.542	1713.333
60	2.376	2640.000

In this case the corrosion rate curve has shown similar behavior as that of SO2. But the rate of corrosion rate is slower in this case

4.2.3 Case at 298K varying the relative humidity

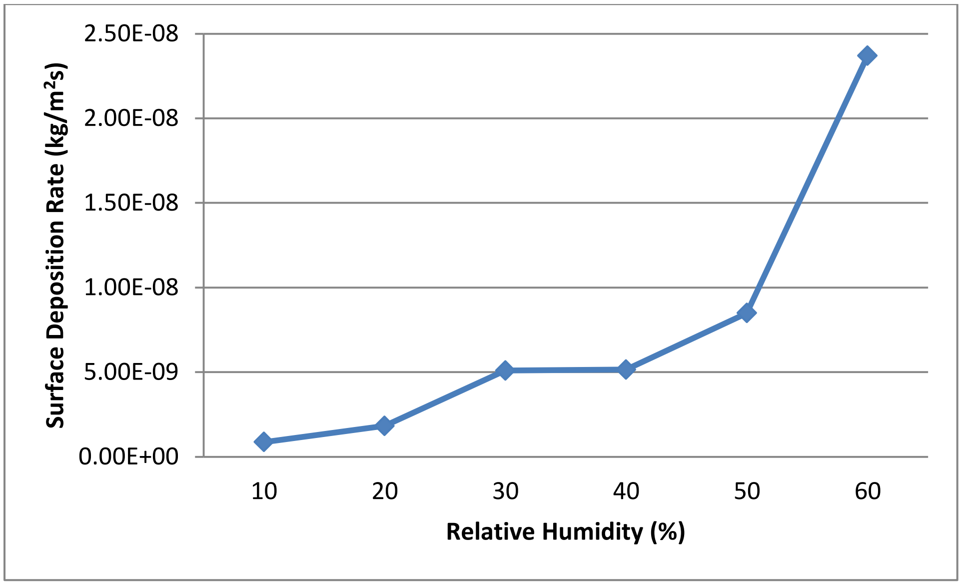

Figure 59 Relative humidity v/s Surface Deposition rate (kg/m2s) at 298K

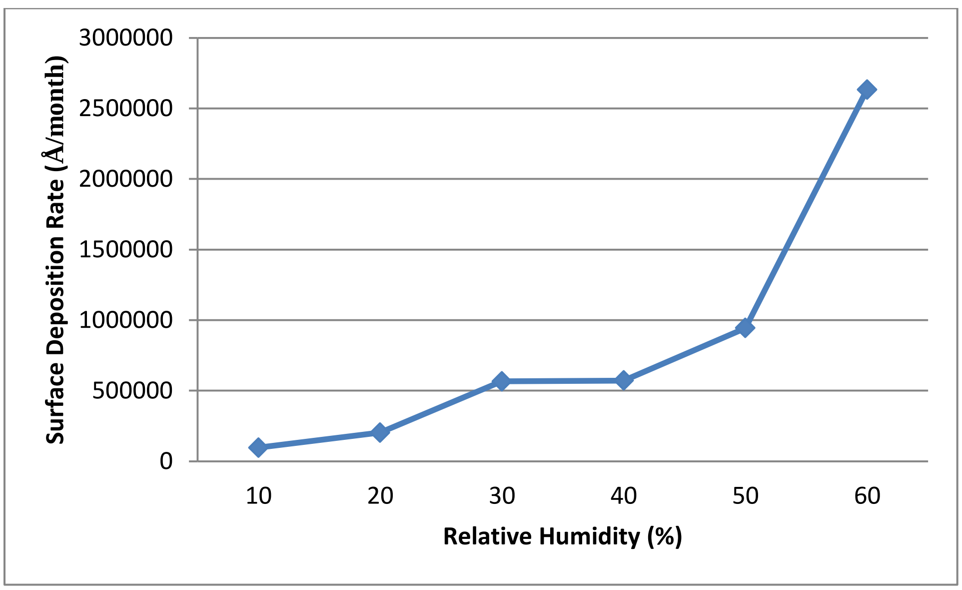

Figure 60 Relative humidity v/s Surface Deposition rate (Å/month) at 298K

Table 21 Surface Deposition Rate at varying RH (at 298K)

Relative Humidity (%)	Surface Deposition Rate $(kg/m^2s)x10^{-9}$	Surface Deposition Rate $(Å/month)x10^3$
10	0.8641	96.011
20	1.825	202.778
30	5.092	565.778
40	5.146	571.778
50	8.488	943.111
60	23.70	2633.333

As seen from the graphs the corrosion rate has steadily increased except for the 30% to 40% RH range where the corrosion did not show considerable increase.

4.2.4 Case at 297K varying the relative humidity

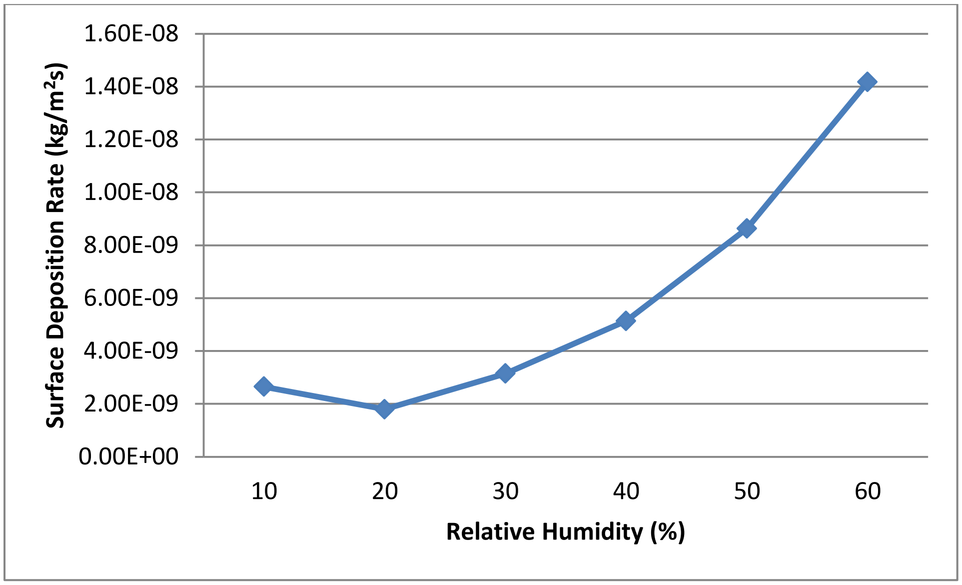

Figure 61 Relative humidity v/s Surface Deposition rate (kg/m2s) at 297K

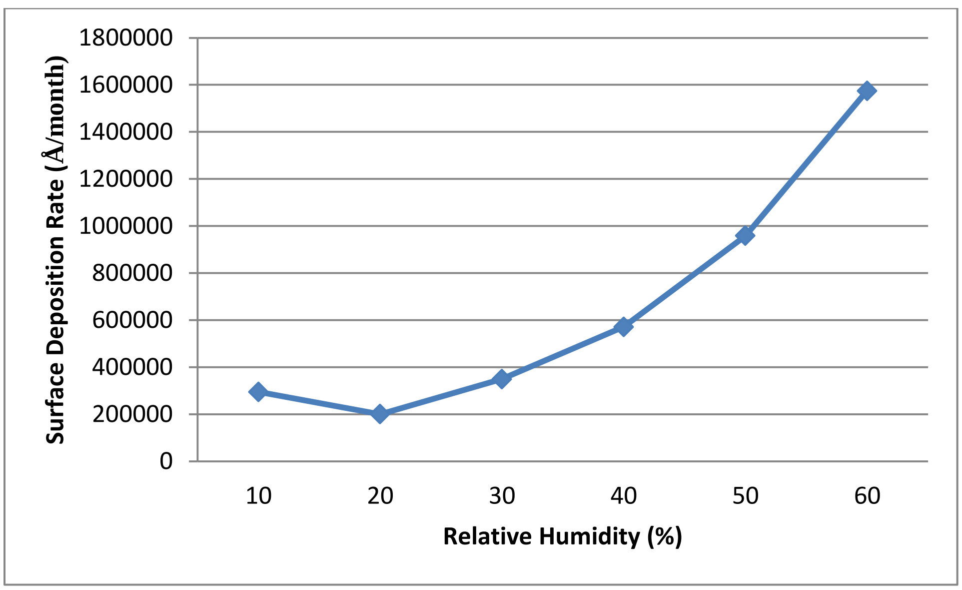

Figure 62 Relative humidity v/s Surface Deposition rate (Å/month) at 297K

Table 22 Surface Deposition Rate at varying RH (at 297K)

Relative Humidity (%)	Surface Deposition Rate (kg/m^{2}s)x10^{-9}	Surface Deposition Rate (Å/month)x10^3
10	2.649	294.333
20	1.797	199.667
30	3.142	349.111
40	5.137	570.778
50	8.626	958.444
60	14.17	1574.444

In this case the corrosion rate went up after the first dip at 20% RH.

4.2.5 Case at 296K varying the relative humidity

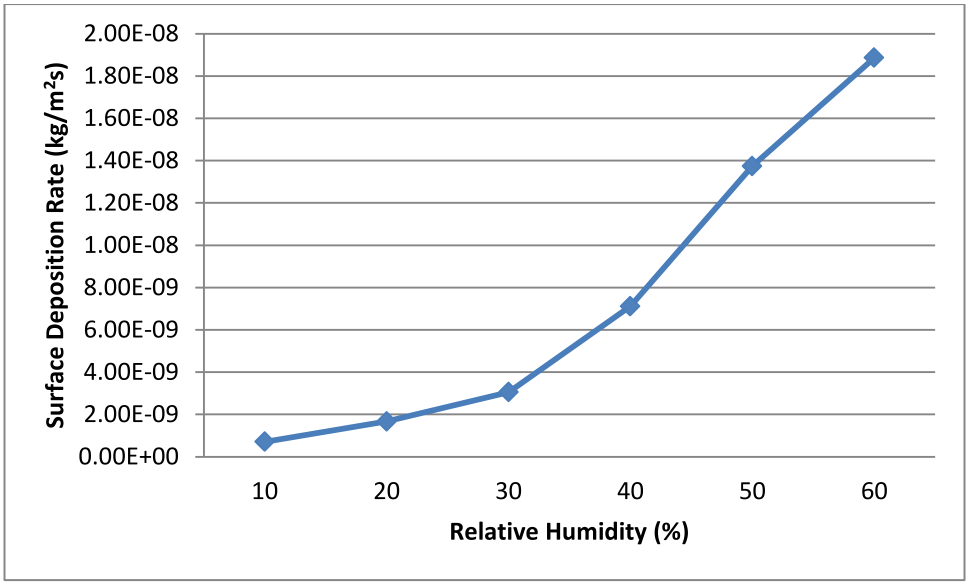

Figure 63 Relative humidity v/s Surface Deposition rate (kg/m2s) at 296K

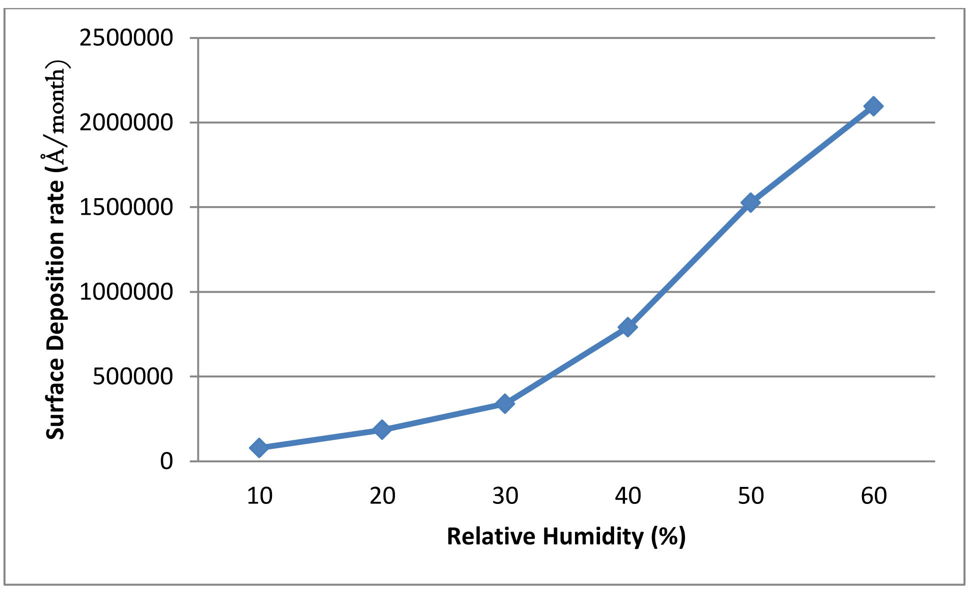

Figure 64 Relative humidity v/s Surface Deposition rate (Å/month) at 296K

Table 23 Surface Deposition Rate at varying RH (at 296K)

Relative Humidity (%)	Surface Deposition Rate (kg/m^{2}s)x10^{-9}	Surface Deposition Rate (Å/month)x10^3
10	0.7050	78.333
20	1.668	185.333
30	3.053	339.222
40	7.118	790.889
50	13.74	1526.667
60	18.86	2095.556

In this case the corrosion rate went up as the relative humidity increased in the controlled volume.

4.2.6 Case at 295K varying the relative humidity

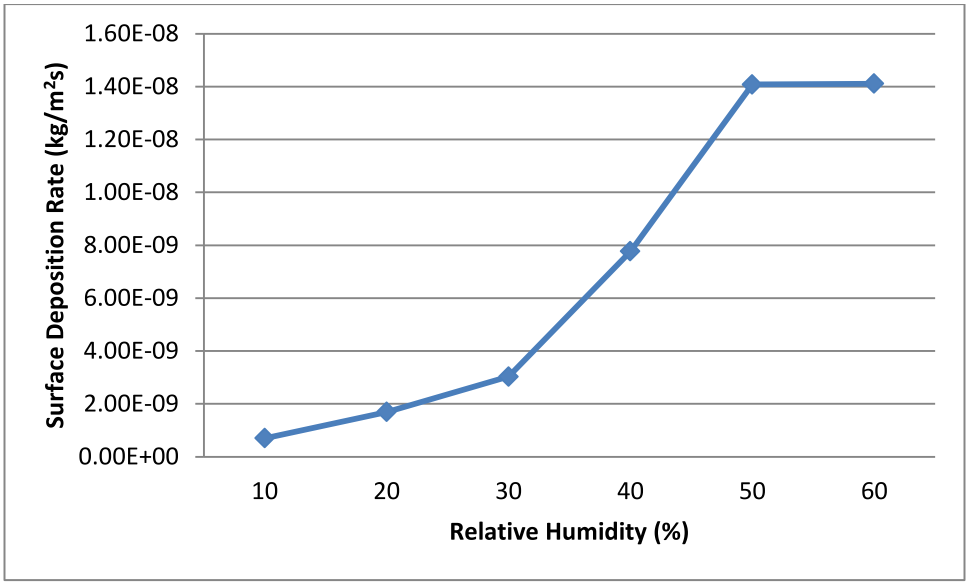

Figure 65 Relative humidity v/s Surface Deposition rate (kg/m2s) at 295K

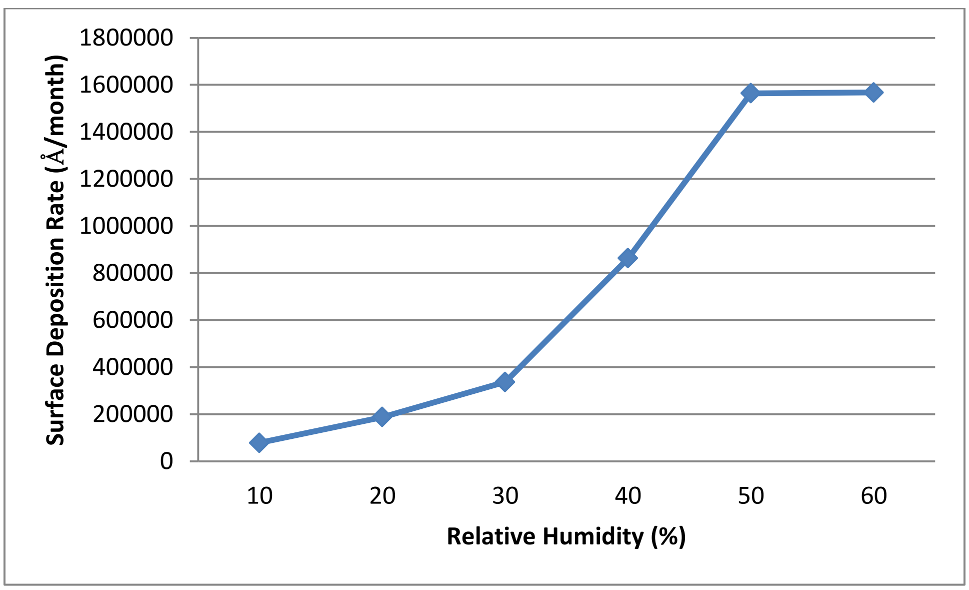

Figure 66 Relative humidity v/s Surface Deposition rate (Å/month) at 295K

Table 24 Surface Deposition Rate at varying RH (at 295K)

Relative Humidity (%)	Surface Deposition Rate (kg/m^2s)x10^{-9}	Surface Deposition Rate (Å/month)x10^3
10	0.7011	77.900
20	1.689	187.667
30	3.032	336.889
40	7.769	863.222
50	14.08	1564.444
60	14.11	1567.778

In this case the corrosion rate has again shown an increase. The last step 50%to 60% the corrosion rate has reduced slope of increment.

4.2.7 Case at 294K varying the relative humidity

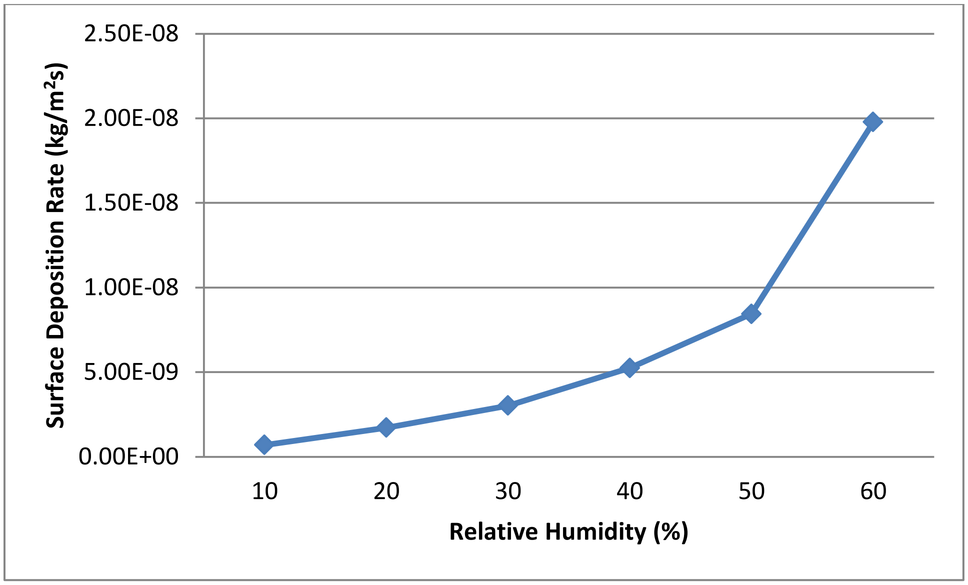

Figure 67 Relative humidity v/s Surface Deposition rate (kg/m2s) at 294K

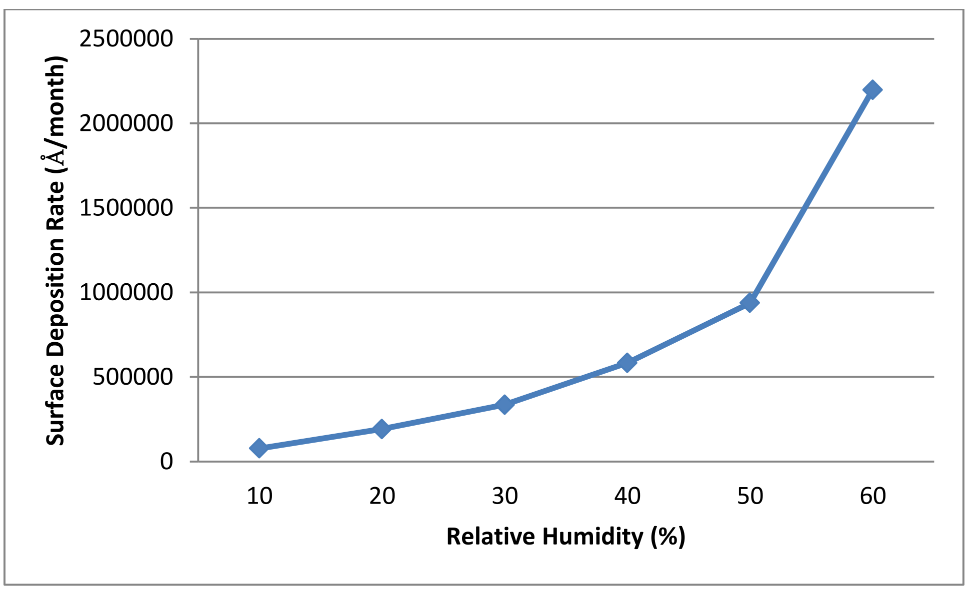

Figure 68 Relative humidity v/s Surface Deposition rate (Å/month) at 294K

Table 25 Surface Deposition Rate at varying RH (at 294K)

Relative Humidity (%)	Surface Deposition Rate (kg/m^{2}s)x10^{-9}	Surface Deposition Rate (Å/month)x10^3
10	0.6935	77.0556
20	1.720	191.111
30	3.017	335.222
40	5.247	583.000
50	8.436	937.333
60	19.78	2197.778

This case has also shown an increase in corrosion rate as the relative humidity increases.

4.2.8 Case at 293K varying the relative humidity

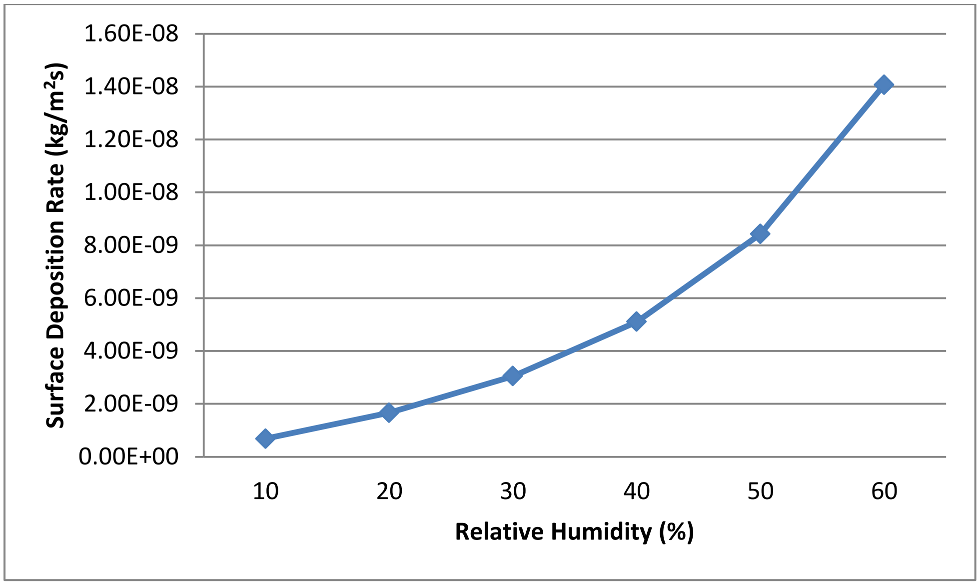

Figure 69 Relative humidity v/s Surface Deposition rate (kg/m2s) at 293K

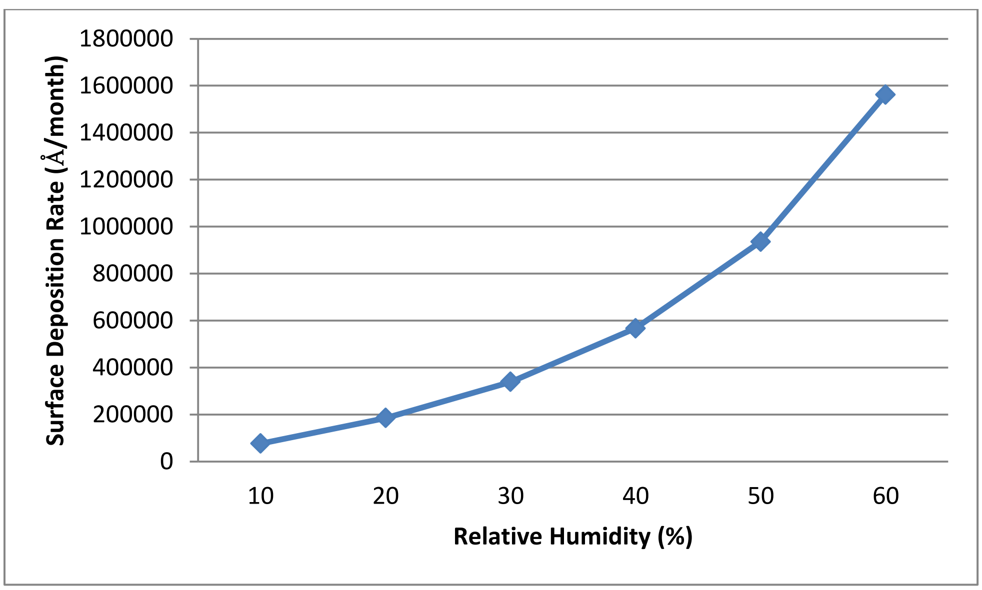

Figure 70 Relative humidity v/s Surface Deposition rate (Å/month) at 293K

Table 26 Surface Deposition Rate at varying RH (at 293K)

Relative Humidity (%)	Surface Deposition Rate (kg/m^2s)x10^{-9}	Surface Deposition Rate (Å/month)x10^3
10	0.6807	75.633
20	1.663	184.778
30	3.049	338.778
40	5.102	566.889
50	8.419	935.444
60	14.06	1562.222

As seen from the graphs the corrosion rate has increased in this case as well, with the increase of relative humidity.

4.2.9 Case at 292K varying the relative humidity

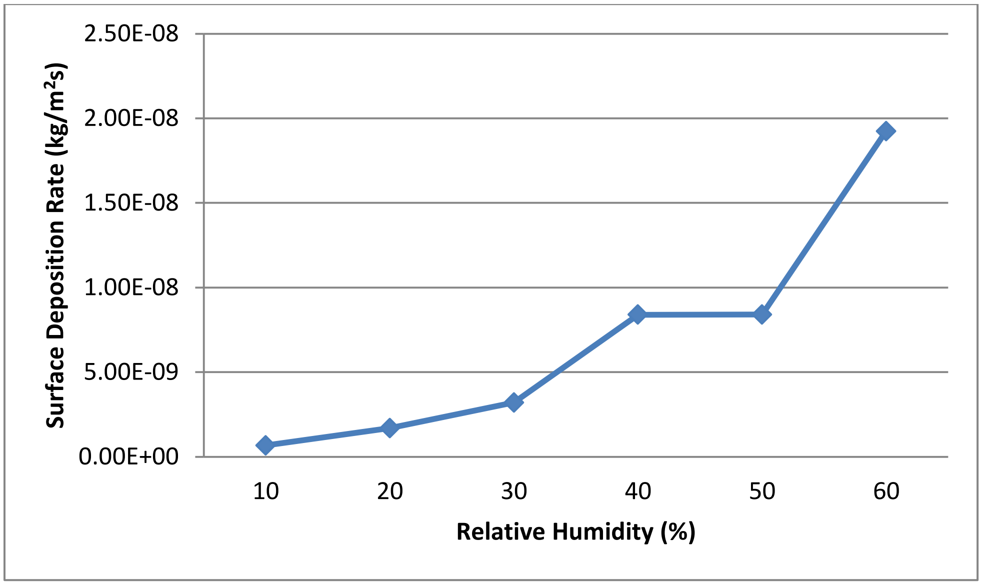

Figure 71 Relative humidity v/s Surface Deposition rate (kg/m2s) at 292K

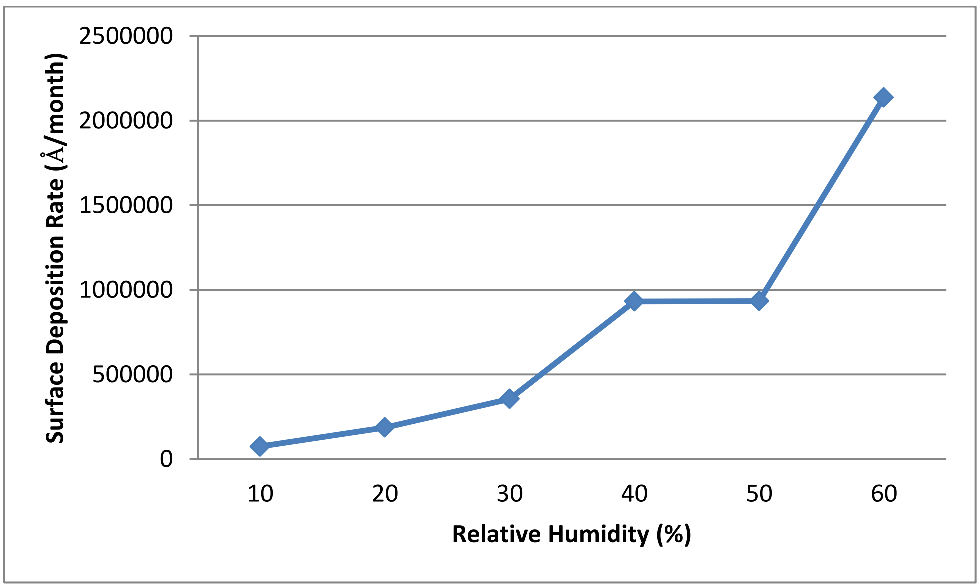

Figure 72 Relative humidity v/s Surface Deposition rate (Å/month) at 292K

Table 27 Surface Deposition Rate at varying RH (at 292K)

Relative Humidity (%)	Surface Deposition Rate $(kg/m^2s) \times 10^{-9}$	Surface Deposition Rate $(Å/month) \times 10^{3}$
10	0.669	74.100
20	1.684	187.111
30	3.197	355.222
40	8.391	932.333
50	8.405	933.889
60	19.24	2137.778

This case had also shown the same trend in its corrosion rate except for the relative humidity range of 30%-40% where the corrosion rate increased at a lower rate as compared to other rates.

This would be the last set of simulations in this section of varying the relative humidity and keeping the temperature constant. As seen from the data of the tables the corrosion rate at a given temperature has not shown a constant trend. This will be studied in the next set of cases.

4.2.10 Case at 60% Relative humidity varying the temperature

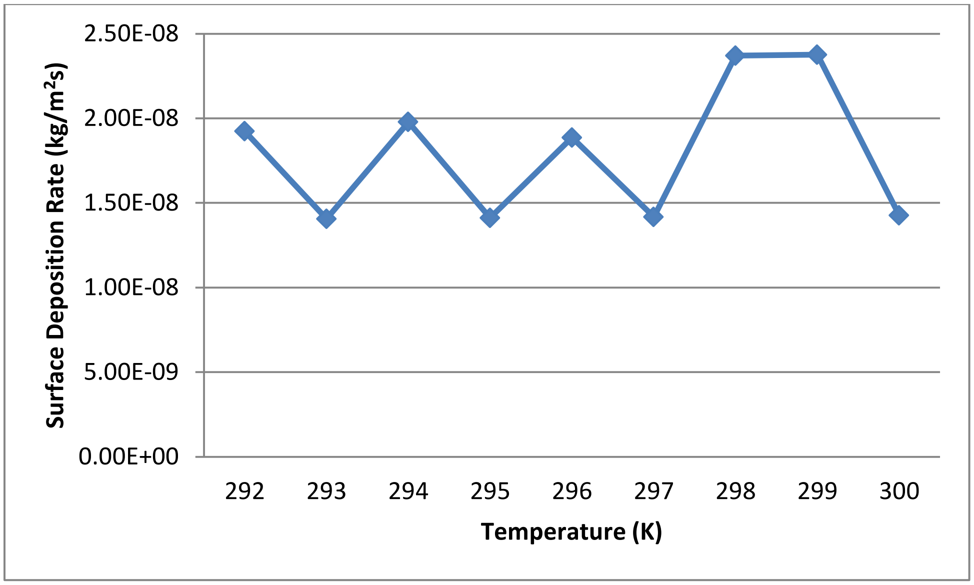

Figure 73 Temperature v/s Surface Deposition rate (kg/m2s) at 60% RH

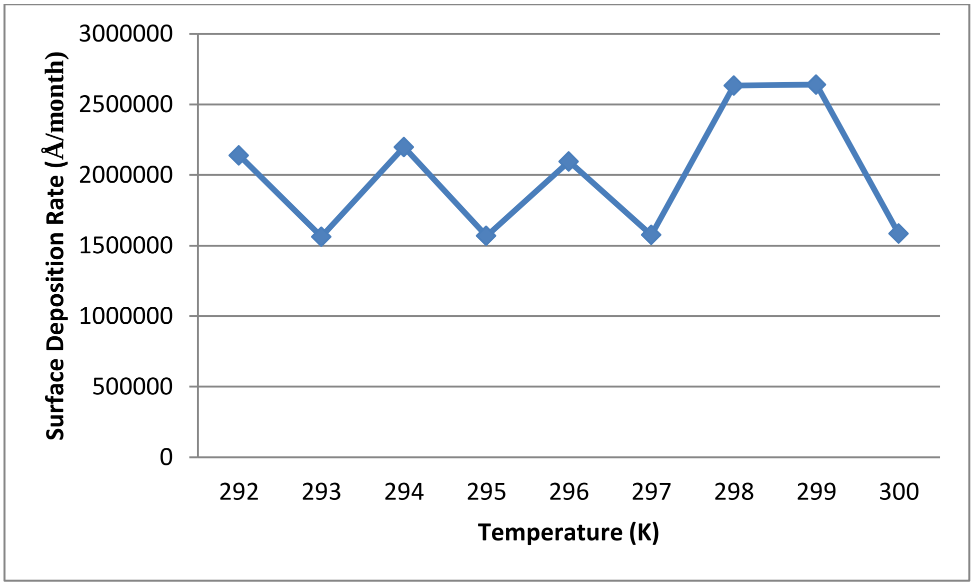

Figure 74 Temperature v/s Surface Deposition rate (Å/month) at 60% RH

Table 28 Surface Deposition Rate at varying Temperature (at 60%RH)

Temperature (K)	Surface Deposition Rate $(kg/m^2s)x10^{-9}$	Surface Deposition Rate $(Å/month)x10^3$
292	19.24	2137.778
293	14.06	1562.222
294	19.78	2197.778
295	14.11	1567.778
296	18.86	2095.556
297	14.17	1574.444
298	23.70	2633.333
299	23.76	2640.000
300	14.25	1583.333

As we can see the corrosion rate has not shown any particular trend as we increased the temperature from 292K-300K. This behavior would have to be studied.

4.2.11 Case at 50% Relative humidity varying the temperature

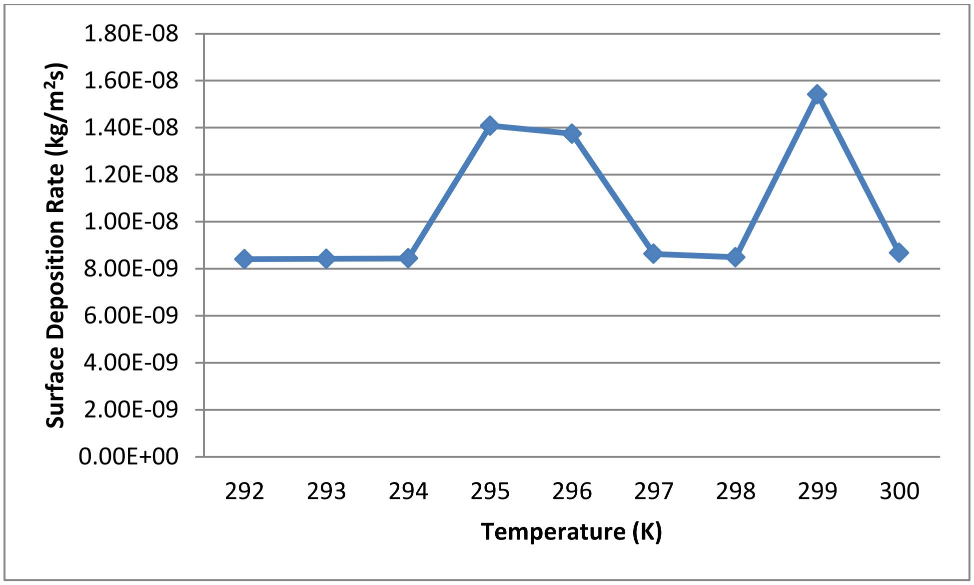

Figure 75 Temperature v/s Surface Deposition rate (kg/m2s) at 50% RH

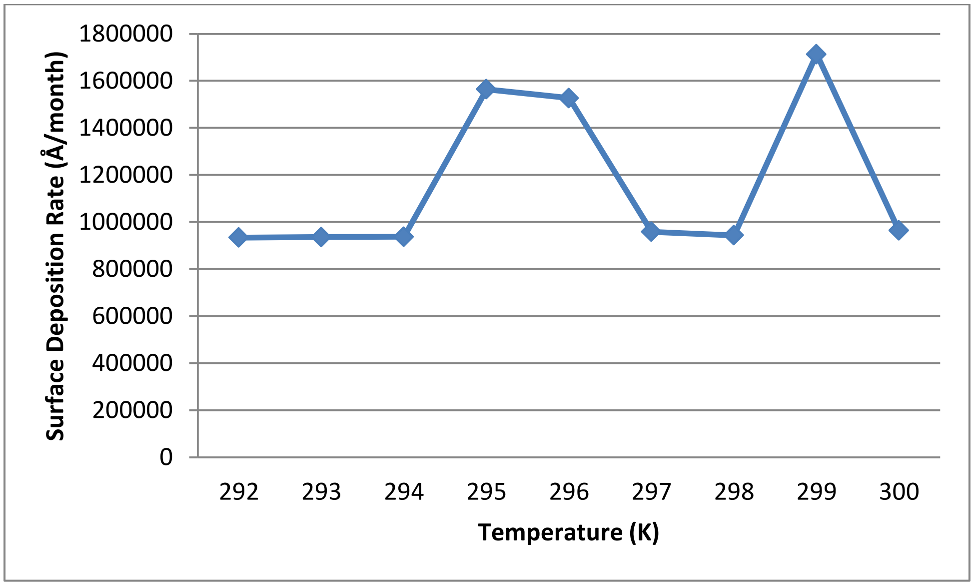

Figure 76 Temperature v/s Surface Deposition rate (Å/month) at 50% RH

Table 29 Surface Deposition Rate at varying Temperature (at 50%RH)

Temperature (K)	Surface Deposition Rate $(kg/m^2s) \times 10^{-9}$	Surface Deposition Rate $(Å/month) \times 10^{3}$
292	8.405	933.889
293	8.419	935.444
294	8.436	937.333
295	14.08	1564.444
296	13.74	1526.667
297	8.626	958.444
298	8.488	943.111
299	15.42	1713.333
300	8.671	963.444

As we increase the temperature from 292K to 300K the irregularities in the corrosion rate rend have decreased but we can still observe at 295K, 296K and 299K that the corrosion rate is high as compared to other temperatures.

4.2.12 Case at 40% Relative humidity varying the temperature

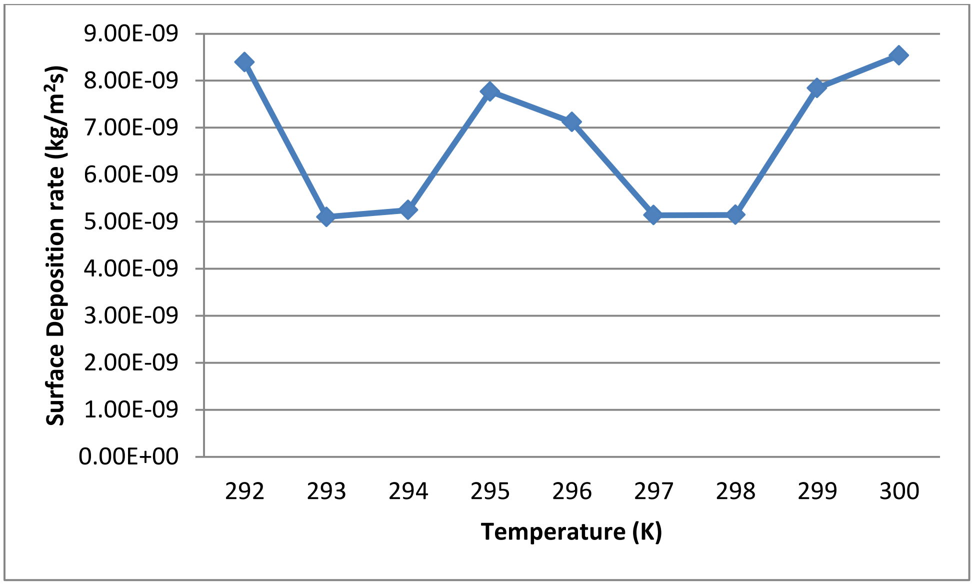

Figure 77 Temperature v/s Surface Deposition rate (kg/m2s) at 40% RH

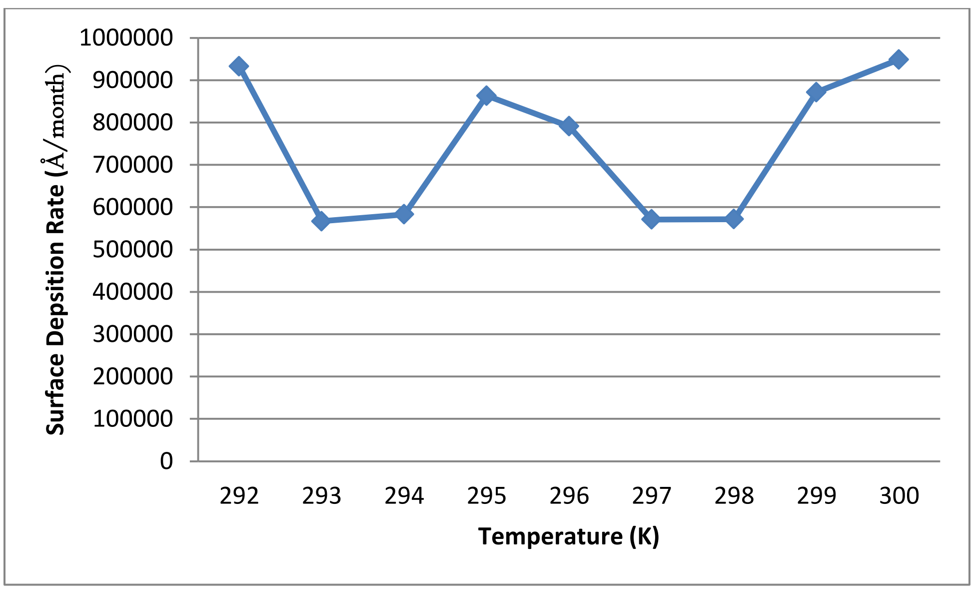

Figure 78 Temperature v/s Surface Deposition rate (Å/month) at 40% RH

Table 30 Surface Deposition Rate at varying Temperature (at 40%RH)

Temperature (K)	Surface Deposition Rate (kg/m^2s)x10^{-9}	Surface Deposition Rate (Å/month)x10^3
292	8.391	932.333
293	5.102	566.889
294	5.247	583.000
295	7.769	863.222
296	7.118	790.889
297	5.137	570.778
298	5.146	571.778
299	7.843	871.444
300	8.538	948.667

As seen again the corrosion rate trend has not shown a set behavior (as we observed in the case of Hydrogen Sulfide).

4.2.13 Case at 30% Relative humidity varying the temperature

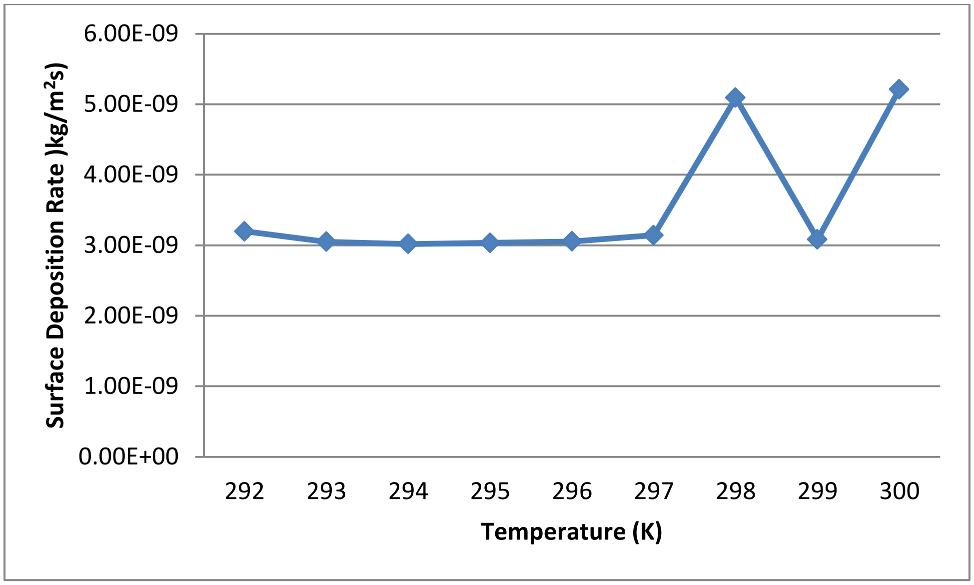

Figure 79 Temperature v/s Surface Deposition rate (kg/m2s) at 30% RH

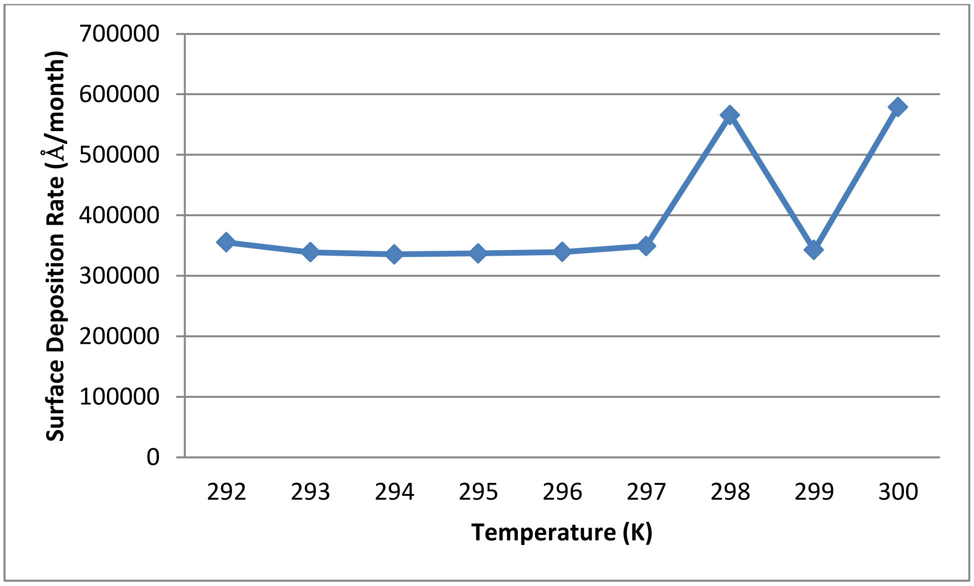

Figure 80 Temperature v/s Surface Deposition rate (Å/month) at 30% RH

Table 31 Surface Deposition Rate at varying Temperature (at 30%RH)

Temperature (K)	Surface Deposition Rate (kg/m^2s)x10^{-9}	Surface Deposition Rate (Å/month)x10^3
292	3.197	355.222
293	3.049	338.778
294	3.017	335.222
295	3.032	336.889
296	3.053	339.222
297	3.142	349.111
298	5.092	565.778
299	3.083	342.556
300	5.209	578.778

As seen from the graphs in this case the corrosion rate show a decrease till 296K but rise thereafter while having a plunge at 299K and rising again.

4.2.14 Case at 20% Relative humidity varying the temperature

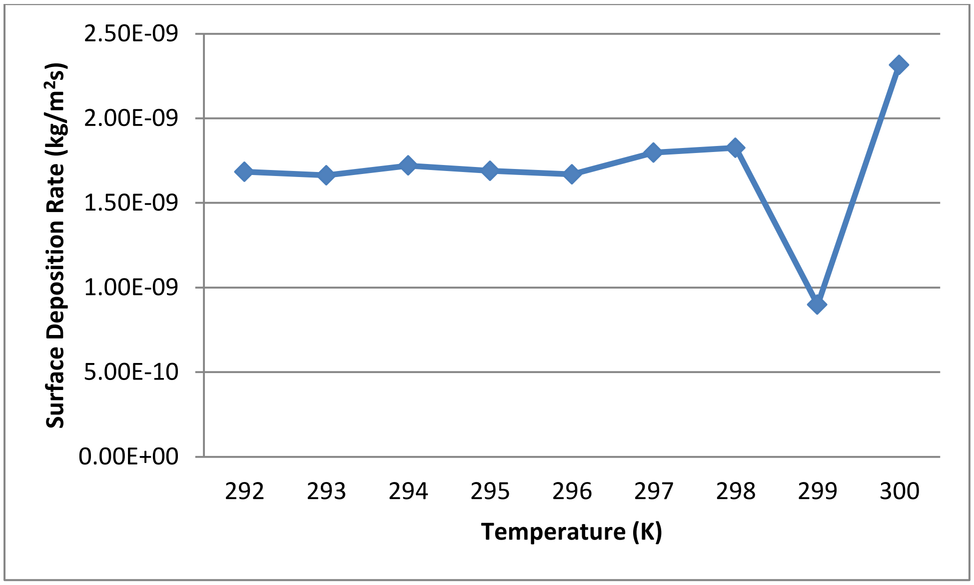

Figure 81 Temperature v/s Surface Deposition rate (kg/m2s) at 20% RH

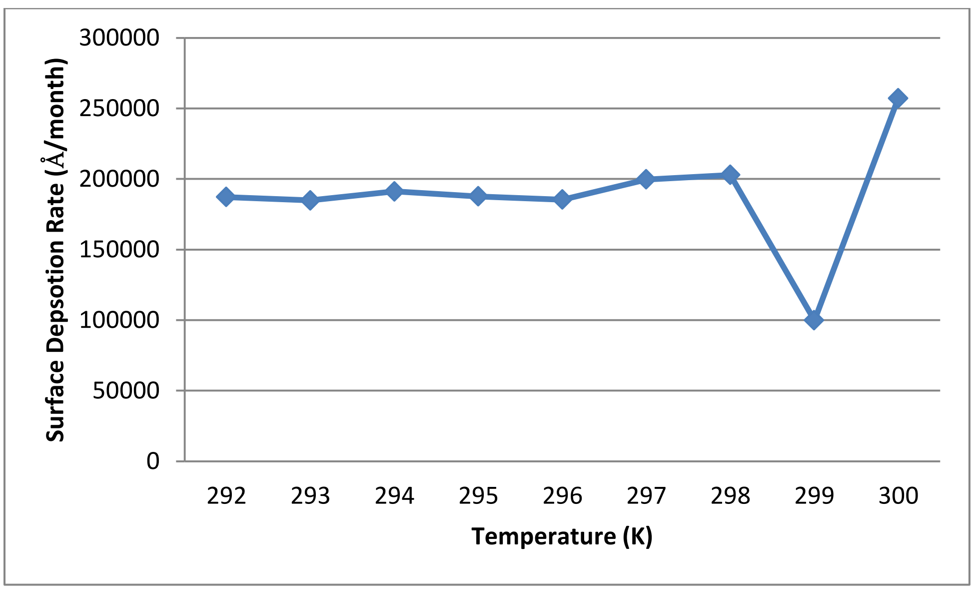

Figure 82 Temperature v/s Surface Deposition rate (Å/month) at 20% RH

Table 32 Surface Deposition Rate at varying Temperature (at 20%RH)

Temperature (K)	Surface Deposition Rate $(kg/m^2s)x10^{-9}$	Surface Deposition Rate $(Å/month)x10^3$
292	1.684	187.111
293	1.663	184.778
294	1.720	191.111
295	1.689	187.667
296	1.668	185.333
297	1.797	199.667
298	1.825	202.778
299	0.898	99.800
300	2.315	257.222

In this case the corrosion rate showed almost a constant rate except at 299K where it plunged down to $99.8x10^3$ Å/month.

4.2.15 Case at 10% Relative humidity varying the temperature

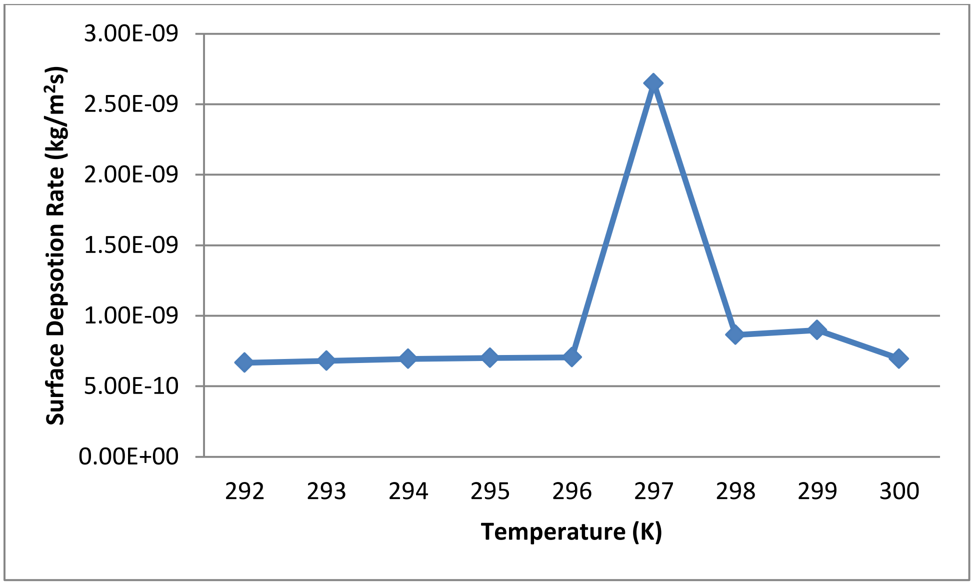

Figure 83 Temperature v/s Surface Deposition rate (kg/m2s) at 10% RH

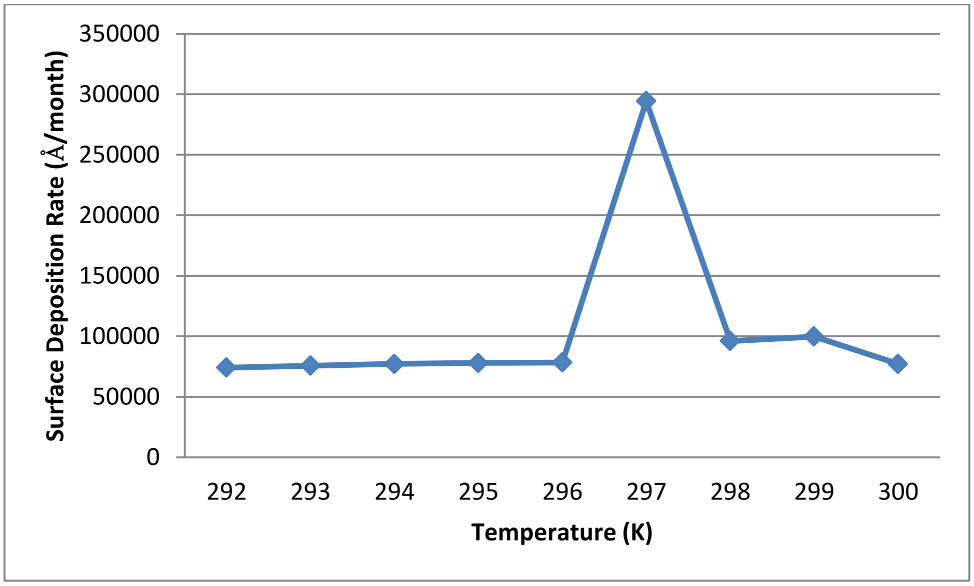

Figure 84 Temperature v/s Surface Deposition rate (Å/month) at 10% RH

Table 33 Surface Deposition Rate at varying Temperature (at 10%RH)

Temperature (K)	Surface Deposition Rate $(kg/m^2s)x10^{-9}$	Surface Deposition Rate $(Å/month)x10^3$
292	0.669	74.100
293	0.680	75.633
294	0.693	77.055
295	0.701	77.900
296	0.705	78.333
297	2.649	294.333
298	0.864	96.01
299	0.898	99.800
300	0.694	77.177

As seen the corrosion rate has again shown an almost constant behavior. At 297K the corrosion rate raised up to $294.333x10^3$ Å/month.

Chapter 5

Conclusion and Future Work

As per the study done the corrosion rate has shown a regular behavior in most of the cases as we increased the Relative Humidity or Temperature. At some of the points that were tested the corrosion rate did not follow the trend. Series of experimental tests that that would follow this thesis study in future would consider these points to test and focus on to check what would be the actual phenomenon behind this trend.

This study focused only on the effects of H_2S and SO_2 on copper. In reality many more gaseous contaminants exists. A study of these contaminants would also be a future study work.

Apart from Copper, Silver is also among the major elements of PCB. A study of how the contaminants have an effect on silver could also be of interest.

Appendix A

Conversion of µg/cm^{2}h to Å/month

The unit kg/m^2-s is first converted into $\mu g/cm^2$-hr and then to convert $\mu g/cm^2$-hr to Å/month following procedure is followed.

Consider copper sulfate (Cu_2S) the only corrosion product with density 5.6 g/cm^3 [4]

$$
\begin{aligned}
1\,\mu g &\equiv \frac{2 \times 63.55 + 32}{32} \mu g \text{ of } Cu_2S \\
&\equiv 5 \times 10^{-6} \text{ g of } Cu_2S \\
&\equiv \frac{5 \times 10^{-6}}{5.6} \text{ cm}^3 \text{of } Cu_2S \\
&\equiv 0.9 \times 10^{-6} \text{ cm}^3 \text{ of } Cu_2S
\end{aligned}
$$

$$
\begin{aligned}
1\ \mu g/cm^2 \cdot h &\equiv 0.9 \times 10^{-6} \text{ cm/h} \\
&\equiv 0.9 \times 10^{-6} \times 10^8 \text{ Å/h} \\
&\equiv 90 \times 24 \times 30 \text{ Å/30 days} \\
&\equiv 6.4 \times 10^4 \text{ Å/30 days}
\end{aligned}
$$

References

[1] CRC Handbook of Chemistry and Physics, 95th Edition

[2] http://epa.gov/climatechange/science/causes.html

[3]http://www.praxairdirect.com/Specialty-Gas-Information-Center/Safety-Information/Flammable-Corrosive-and-Toxic-Gases.html

[4] 2011Gaseous and Particulate Contamination guidelines for data centers by ASHRAE

[5] 2005 ASHRAE Handbook – Fundamentals (Chapter9. Indoor Environment Health)

[6] "Impact of dust on Printed Circuit Assembly Reliability"; Bo Song, Michael H. Azarian & Michael G. Pecht, Center of Advanced Life Cycle Engineering (CALCE), University of Maryland, College Park, MD

[7] "Design Guidelines for the Assessment, Control, and testing of Gaseous Contamination in Data Centers and Server Rooms" by Purafil

[8] "Corrosion Costs and Preventive Strategies in the United States" by National Association of Corrosion (NACE) international

[9] White paper "Global Needs for Knowledge Dissemination, Research, and Development in Materials Deteriotion and Corrosion Control" by Gunter Schmitt (The World Corrosion Organization)

[10]http://chemwiki.ucdavis.edu/Analytical_Chemistry/Electrochemistry/Case_Studies/Corrosion

[11]http://www.datacenterdynamics.com/focus/archive/2013/06/evolution-design-and-data-center-cooling

[12] https://www.workspace-technology.com/products-services/data-centre-design-and-build-data-centre-solutions/server-room-cooling-airflow-management/freecool-evaporative-free-air-cooling-technology-overview/

[13] http://www.epa.gov/iaq/pubs/residair.html

[14] SULTZ Solutions and Services Boucher QC-SAT0070

[15] DIRECTIVE 2002/95/EC OF THE EUROPEAN PARLIAMENT AND OF THE COUNCIL of 27 January 2003 on the restriction of the use of certain hazardous substances in electrical and electronic equipment

[16] http://www.shinko.co.jp/english/product/leadframe/

[17] http://www.webelements.com/copper/

[18] http://www.webelements.com/silver/

[19] Testing Printed Circuit Boards for Creep Corrosion in Flowers of Sulfur Chamber, Parabjit Singh, IBM; Et. al

[20] "Case Study of Printed Circuit Board Corrosion and Countermeasures" NTT EAST Ota-ku, 144-0053 Japan

[21]http://chemwiki.ucdavis.edu/Analytical_Chemistry/Electrochemistry/Case_Studies/Corrosion

[22] http://corrosion.ksc.nasa.gov/corr_forms.htm

[23] “The Influence of Oxide Layers on Initial Corrosion behavior of Copper in air containing water vapor and sulfur dioxide” by Jun Itoh, Takeshi Sasaki, Toshiaki Ohtsuka from Hokkaido University, Japan

[24] “Development of a detailed computational model of high end servers and validating using experimental methods” Vijayalayan Pandiya, 2013

[25] http://www.engineeringtoolbox.com/laminar-transitional-turbulent-flow-d_577.html

[26] http://blog.nialbarker.com/252/slow_is_faster

[27] “The numerical computation of turbulent flows” B.E. Launder, D.B. Spalding; Appendix D – Computer methods in Applied Mechanics and engineering 1974

[30] “Low Reynolds Number Turbulence Models for accurate Thermal Simulations of electronic components” K.K. Dhanisa, C.J.Bailey, K.A. Pericleous; International Conference of Thermal and Mechanical Simulation and experiments in Micro-Electronics, EuroSimE; 2004

[31] ANSYS Fluent Tutorial Guide, ANSYS Inc.

[32] ANSYS Theory guide, ANSYS Inc

[33] “Perry’s Standard Tables and Formulae for Chemical Engineers” James Speight; McGraw-Hill Education

Biographical Information

Tejeshkumar Vasantrao Bagul received his Bachelor of Engineering degree in Mechanical Engineering from the University of Pune, India. Tejeshkumar has completed his Masters in Engineering degree in Mechanical Engineering from the University of Texas at Arlington, USA in December 2014.

Tejeshkumar has always been interested in Computational Fluid Dynamics, HVAC systems and Machine design. He has worked in various fields from manufacturing to renewable energy resources to thermal engineering.

Born a leader Tejeshkumar has always aspired to be an entrepreneur in the field of mechanical engineering. He would like to use this knowledge of his in mechanical engineering for the good of mankind and help all the public equally.